Received: 25 February 2021 | Revised: 5 May 2021 | Accepted: 24 May 2021

DOI: 10.1002/rnc.5641

SPECIAL ISSUE ARTICLE

WILEY

Finite-time formation control and obstacle avoidance of multi-agent system with application

Yingxin Shou[1,2] | **Bin Xu**[1] | **Haibo Lu**[2] | **Aidong Zhang**[2] | **Tao Mei**[2]

[1]School of Automation, Northwestern Polytechnical University, Xi'an, China

[2]Peng Cheng Laboratory, Shenzhen, China

Correspondence
Bin Xu, School of Automation, Northwestern Polytechnical University, Xi'an, Shannxi 710072, China.
Email: smileface.binxu@gmail.com

Funding information
National Natural Science Foundation of China, Grant/Award Number: 61933010, 62003180; Science and Technology on Space Intelligent Control Laboratory, Grant/Award Number: HTKJ2020KL502005

Abstract

The finite-time formation tracking control is investigated for a multi-agent system (MAS) with obstacle avoidance. For the collision and obstacle avoidance problem in the formation process, the artificial potential field is used as the formation planning design, and the virtual structure is adopted to improve the organizational ability of the formation. The trajectory tracking control follows the back-stepping scheme, and the finite-time technique is developed in the control design. Considering the dynamics uncertainty of the agent system, a neural network is applied for estimating and the prediction error-based adaptive law is established to achieve the precise estimation performance. Moreover, the predefined performance function is embedded to satisfy the output constraint. The uniformly ultimate boundedness of the system error signals and the finite-time convergence of the MAS are guaranteed. The simulation study is performed to validate the proposed control for multiple autonomous underwater vehicles system, while the results manifest that the obstacle avoidance with high-precision tracking and formation performance will be achieved under the formation trajectory tracking controller.

KEYWORDS

finite-time convergence, formation obstacle avoidance control, multi-agent system, multi-autonomous underwater vehicles system, neural network, predefined performance function

1 | INTRODUCTION

The multi-agent system (MAS) refers to a system composed of multiple agents, such as multi-autonomous underwater vehicles (multi-AUV) system, multi-unmanned aerial vehicle system, multi-robot system, and so forth. The agents in the system coordinate with each other to complete tasks such as area search, terrain scanning, and environmental data collection. Many scholars have conducted studies[1-5] on coordinated allocation, trajectory planning, coordinated decision, and coordinated control. To obtain precise operating performance, coordinated control as an essential part has been extensively studied. One of the key aspects related to coordinated control is the formation control of multiple agents in performing operative tasks.

Various strategies have been studied for the formation control of the MAS, including leader-following,[6] virtual structure,[7] and behavior control.[8] In the leader-follower control strategy, the leader moves along a specified path according to the task or real-time instructions, the followers track the leader with a certain position offset by acquiring the leader's status information, thereby forming a certain formation. However, since the entire MAS lacks feedback information the control system will be completely restrained by the leader. The virtual structure control strategy regards agents

as a virtual rigid structure and derives the motion state information of each virtual structure point (VSP) according to the system's motion dynamic model. The target tracking algorithm is designed to make the position converge to the corresponding VSP. The behavior control strategy decomposes the agent's tasks into multiple basic behaviors and designs the weighted fusion control output to achieve formation control. Overall, due to the lack of flexibility and adaptability of the above methods, it is difficult to deal with relatively complex application scenarios especially the tasks with obstacles.

The formation control strategy based on the artificial potential field (APF) is introduced for obstacle avoidance. A virtual potential field (PF) is set in the working space of the agent, and the agent moves along the negative gradient direction of the PF under the action of the PF force. The disadvantage of the APF method is that it is not flexible enough, which because the change of formation requires the reconfiguration of the PF function. In Reference 9, the method of combining the virtual agent and APF is applied to generate the reference trajectory of the position, formation of the virtual agent is controlled by changing the PF shape. In Reference 10, APF is arranged in the shape of a "groove", and the agents move into the "groove" to form the formation. The changes of different formations require different forms of "grooves". It can be seen that the arrangement of formations using APF is actually not easy. Taking into account the strong formation organization ability of the virtual structure method and the obstacle avoidance ability of the APF method, the compound coordinated control strategy is proposed in Reference 11. Through the established VSPs, the formation reference point (FRP) and target reference point (TRP) of the sports space are formed, and the preset formation is obtained. The APF between the TRP and the FRP is established, the multiple agents follow the VSP to the desired position under the action of the PF.

Considering the nonlinear dynamics and uncertainty of MAS, a variety of control technologies have been extensively studied, such as backstepping control,[12] nonlinear adaptive control,[13] robust control,[14] intelligent control,[15] and so forth. A distributed cooperative learning control is proposed with the dynamics uncertainty approximation,[16] and a robust sliding mode control is designed with the estimated upper bound of uncertainty.[17] Neural network (NN)[18,19] is reported due to the ability to approximate the nonlinearity without the linearized parameter model. The NN learning technology can be used to estimate and compensate for the disturbance, and a neural adaptive protocol is proposed for the heterogeneous switched MAS in Reference 20. Furthermore, the motivation using the intelligent technology to estimate the nonlinearity is considered, the tracking precision is greatly improved. In Reference 21, the neural control with serial-parallel estimation model (SPEM) is designed and the learning performance index is extracted. An online data-based composite neural controller is proposed in Reference 22, and the prediction error is established with the collected data and the error dynamics.

As for the closed-loop convergence in the control design, the asymptotic stability technique and the finite-time convergence technique are useful properties.[23,24] Since the prescribed performance of system tracking is desired in many engineering systems, the system states are in demand.[25] In Reference 26, the barrier Lyapunov function (BLF) is applied to guarantee the desired performance specification, and the finite-time state constraint is designed with the BLF in Reference 27. It is important to interact the finite-time convergence and the predefined performance technology with the neural learning strategy.

In the article, the obstacle avoidance and finite-time formation control with neural learning are studied for the uncertain MAS. Compared with the previous works,[11,28] the contributions are listed as follows:

(1) The coordinated adaptive controller based on virtual structure and APF is designed to realize obstacle avoidance and formation track. With the TRP as the center, the FRP is generated based on the virtual structure method, and the APF repulsion functions between the FRPs are constructed to realize the formation avoidance.
(2) The finite-time back-stepping control with finite-time filter is designed to guarantee the finite-time ultimate uniformly bounded (UUB) stability. Furthermore, the predefined performance control is adopted to ensure that the system output is restricted by the predefined performance.
(3) The prediction error-based neural control is proposed to estimate the dynamics uncertainty of the agents, and the finite-time SPEM is established to extract the learning performance index. The simulation test on the multi-AUV system shows that the effective control performance under the proposed controller.

The organization of this article is shown as follows. The system dynamics and the preliminaries are described in Section 2. The formation planning design and the control design are performed in Sections 3and 4, respectively. The system stability is analyzed in Section 5, and the simulation is illustrated in Section 6. The conclusions are described in Section 7.

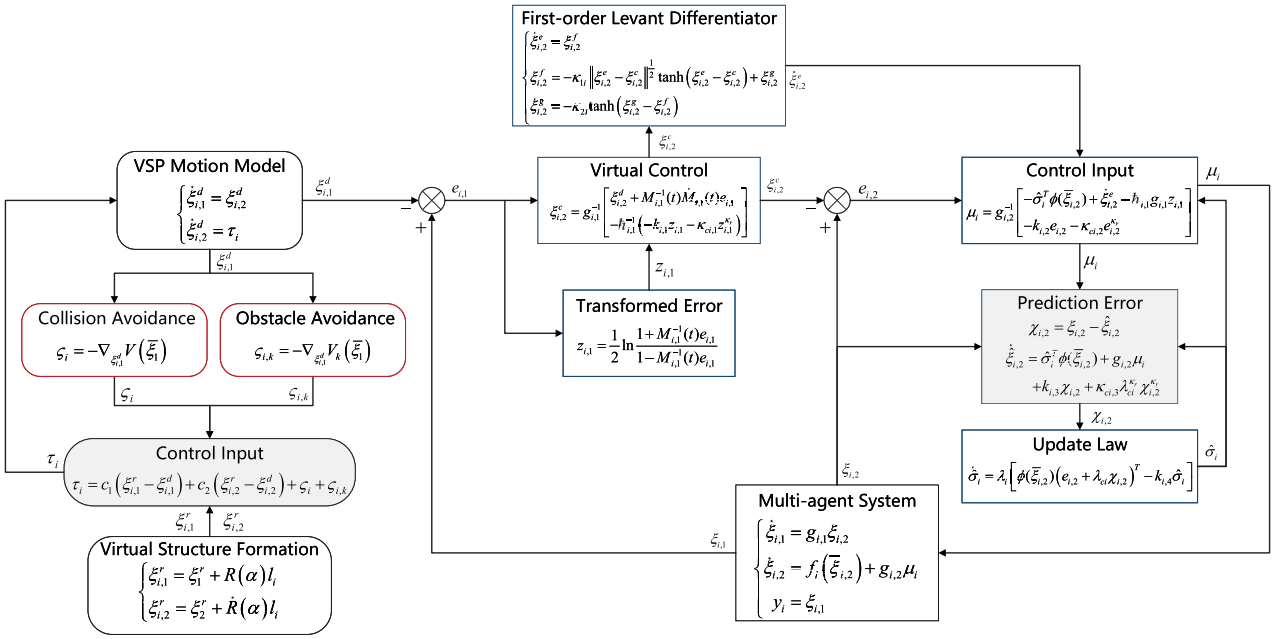

FIGURE 1 Control scheme [Colour figure can be viewed at wileyonlinelibrary.com]

2 | SYSTEM DYNAMICS AND PRELIMINARIES

2.1 | System dynamics

The dynamics of the MAS is considered as follows:

$$\begin{cases} \dot{\boldsymbol{\xi}}_{i,1} = \boldsymbol{g}_{i,1}\boldsymbol{\xi}_{i,2} \\ \dot{\boldsymbol{\xi}}_{i,2} = \boldsymbol{f}_i\left(\overline{\boldsymbol{\xi}}_{i,2}\right) + \boldsymbol{g}_{i,2}\boldsymbol{\mu}_i \\ \boldsymbol{y}_i = \boldsymbol{\xi}_{i,1} \end{cases} \tag{1}$$

where $\overline{\boldsymbol{\xi}}_{i,2} = \left[\boldsymbol{\xi}_{i,1}^T, \boldsymbol{\xi}_{i,2}^T\right]^T$, $\boldsymbol{\xi}_{i,1} \in \mathfrak{R}^n$ and $\boldsymbol{\xi}_{i,2} \in \mathfrak{R}^n$ are the system states, $\boldsymbol{\mu}_i \in \mathfrak{R}^n$ is the control input, $\boldsymbol{y}_i \in \mathfrak{R}^n$ is the system output, $\boldsymbol{f}_i\left(\overline{\boldsymbol{\xi}}_{i,2}\right)$ is the unknown system uncertainty, $\boldsymbol{g}_{i,1}$ and $\boldsymbol{g}_{i,2}$ are the known control gain functions, $i = 1, \ldots, N$, N is the number of agents, and n is the dimensionality of system.

2.2 | Control goal and control scheme

The control goal is to propose the composite adaptive formation control and obstacle avoidance for the MAS to drive the system output to track the desired trajectory with the certain formation in a finite time. The virtual structure and APF methods are applied for formation avoidance and the prediction error-based neural scheme is designed as an uncertainty approximation method. Figure 1 manifests the control scheme.

2.3 | Preliminaries

Lemma 1. [29] *For the nonlinear system* $\dot{\mathrm{X}} = f(\mathrm{X})$, *a nonnegative Lyapunov function* $\mathcal{V}(\mathrm{X})$ *exists*

$$\dot{\mathcal{V}}(\mathrm{X}) \leq -a_1\mathcal{V}(\mathrm{X}) - a_2\mathcal{V}^b(\mathrm{X}) + \mathcal{V}_l \tag{2}$$

where $a_1 > 0$, $a_2 > 0$, $0 < b < 1$ *are positive parameters, and* $\mathcal{V}_l > 0$.

The system $\dot{\mathrm{X}} = f(\mathrm{X})$ *is finite-time stable, and the residual set is calculated as*

$$\mathcal{V}(\mathrm{X}) \leq \min\left\{\frac{\mathcal{V}_l}{\left(1-\kappa_{\theta_0}\right)a_1}, \left[\frac{\mathcal{V}_l}{\left(1-\kappa_{\theta_0}\right)a_2}\right]^{\frac{1}{b}}\right\} \tag{3}$$

with the settling time as

$$T(\mathrm{X}) \leq \left\{ t_0 + \frac{1}{\kappa_{\theta_0} a_1 (1-b)} \ln \frac{\kappa_{\theta_0} a_1 \mathcal{V}^{1-b}(t_0) + a_2}{a_2}, \right. \\ \left. t_0 + \frac{1}{a_1 (1-b)} \ln \frac{a_1 \mathcal{V}^{1-b}(t_0) + \kappa_{\theta_0} a_2}{\kappa_{\theta_0} a_2} \right\} \tag{4}$$

where $0 < \kappa_{\theta_0} < 1$ *is a positive parameter*.

Lemma 2. *For any positive variables* $\mathrm{X} > 0$, $0 < a < 1$, *and* $c > 0$, *it holds*

$$\begin{cases} c\mathrm{X}^a - \mathrm{X} \leq c - \mathrm{X} \leq c, & \text{if } 0 < X < 1 \\ c\mathrm{X}^a - \mathrm{X} \leq 0, & \text{if } X \geq 1 \end{cases} \tag{5}$$

Remark 1. The unknown dynamics uncertainty is estimated by the radial basis function (RBF) NN[30] as

$$\boldsymbol{f}_i = \boldsymbol{\sigma}_i^{*T} \boldsymbol{\phi}(\bar{\xi}_{i,2}) + \boldsymbol{\varepsilon}_i \tag{6}$$

$$\phi_j = \frac{1}{\sqrt{2\pi} J_{i,j}} \exp\left[-\frac{\left(\bar{\xi}_{i,2} - \boldsymbol{\ell}_{i,j}\right)^T \left(\bar{\xi}_{i,2} - \boldsymbol{\ell}_{i,j}\right)}{2 J_{i,j}} \right] \tag{7}$$

where $\boldsymbol{\sigma}_i^* \in \mathfrak{R}^{\iota_{hi} \times n}$ is the optimal weight, $\boldsymbol{\phi}(\bar{\xi}_{i,2}) = \left[\phi_1, \ldots, \phi_{\iota_{hi}}\right]^T \in \mathfrak{R}^{\iota_{hi} \times 1}$ is the basis function, ι_{hi} is the number of neuron nodes, $\boldsymbol{\ell}_{i,j} \in \mathfrak{R}^{2n}$ is the center point, $J_{i,j} \in \mathfrak{R}$ is the width, $j = 1, \ldots, \iota_{hi}$, $\boldsymbol{\varepsilon}_i \in \mathfrak{R}^n$ is the construction error, and $\|\boldsymbol{\varepsilon}_i\| \leq \bar{\varepsilon}_i$.

3 | FORMATION PLANING DESIGN

In this section, the multi-agent formation algorithm based on virtual structure and APF is proposed to provide the reference signal $\xi_{i,1}^d$ of each agent. The TRP is used as the center of the formation, and the FRP is formed around the TRP as the desired location of the VSP according to the required virtual structure stratum. At the initial moment, multiple agents are randomly distributed and the VSPs move to the desired FRP. During the movement, the APF is set with the VSP as the center to realize collision avoidance and obstacle avoidance.

3.1 | Virtual structure based formation transformation

Define the desired signals of system states as ξ_1^r and ξ_2^r. The desired virtual structure formation is formed as

$$\begin{cases} \xi_{i,1}^{020r} = \xi_1^r + \boldsymbol{R}(\alpha)\boldsymbol{l}_i \\ \xi_{i,2}^r = \xi_2^r + \dot{\boldsymbol{R}}(\alpha)\boldsymbol{l}_i \end{cases} \tag{8}$$

where $\boldsymbol{R}(\alpha) = \begin{bmatrix} \cos\alpha & -\sin\alpha \\ \sin\alpha & \cos\alpha \end{bmatrix}$, α is the angle between the coordinate systems, $\boldsymbol{l}_i$ is the relative position representing the shape of the virtual structure.

3.2 | Virtual structural particle

The motion model of the VSP is described as

$$\begin{cases} \dot{\xi}_{i,1}^{d} = \xi_{i,2}^{d} \\ \dot{\xi}_{i,2}^{d} = \boldsymbol{\tau}_i \end{cases} \tag{9}$$

where $\xi_{i,1}^{d} \in \mathfrak{R}^n$ and $\xi_{i,2}^{d} \in \mathfrak{R}^n$ are the states of the ith particle, $\boldsymbol{\tau}_i \in \mathfrak{R}^n$ is the input of the ith particle.

The input $\boldsymbol{\tau}_i$ is designed as

$$\boldsymbol{\tau}_i = c_1 \left(\xi_{i,1}^{r} - \xi_{i,1}^{d}\right) + c_2 \left(\xi_{i,2}^{r} - \xi_{i,2}^{d}\right) + \varsigma_i + \varsigma_{i,k} \tag{10}$$

where $c_1 > 0$ and $c_2 > 0$ are the design parameters, ς_i is the control item for particle collision avoidance, $\varsigma_{i,k}$ is the control item for formation obstacle avoidance, $k = 1, \ldots, N_1$, and N_1 is the obstacle number.

3.3 | Collision avoidance control between formations

The ith particle is in the PF generated by other particles nearby. The total potential energy of the ith particle can be expressed as

$$\varsigma_i = -\nabla_{\xi_{i,1}^{d}} V\left(\bar{\xi}_1\right) \tag{11}$$

$$V\left(\bar{\xi}_1\right) = \sum_{j \neq i}^{N} \varphi\left(\|\xi_{j,1}^{d} - \xi_{i,1}^{d}\|\right) \tag{12}$$

where $\nabla_{\xi_{i,1}^{d}}$ is the negative gradient term, $\varphi(\mathrm{X})$ is the potential energy function,

$$\varphi(\mathrm{X}) = \begin{cases} \frac{1}{2} k_{\varsigma} \left(\frac{1}{\mathrm{X}} - \frac{1}{R_{\varsigma}}\right), & 0 < \mathrm{X} \leq R_{\varsigma} \\ 0, & \mathrm{X} > R_{\varsigma} \end{cases} \tag{13}$$

with the PF strength coefficient $k_{\varsigma} > 0$, and the radius of the PF $R_{\varsigma} > 0$.

3.4 | Formation avoidance control

The obstacle avoidance area is defined in R_k near the kth obstacle. When the particle is close to the obstacle, the coordinates of the projection point on the obstacle avoidance area are defined as

$$\xi_{i,k,1}^{d} = \boldsymbol{O}_k + R_k \frac{\left(\xi_{i,1}^{d} - \boldsymbol{O}_k\right)}{\|\xi_{i,1}^{d} - \boldsymbol{O}_k\|} \tag{14}$$

where $\boldsymbol{O}_k \in \mathfrak{R}^n$ is the state of the obstacle.

The formation avoidance control is designed as

$$\varsigma_{i,k} = -\nabla_{\xi_{i,1}^{d}} V_k\left(\bar{\xi}_1\right) \tag{15}$$

$$V_k\left(\bar{\xi}_1\right) = \sum_{k=1}^{N_1} \varphi\left(\|\xi_{i,k,1}^{d} - \xi_{i,1}^{d}\|\right) \tag{16}$$

Remark 2. The energy of the APF in (13) is constructed as a function of the relative distance. The negative gradient term of APF energy $\varphi(\mathrm{X})$ causes the particle to move in the direction where the APF energy is reduced, which avoids collision.

Remark 3. By balancing the relationship between the inertia of the multi-agent and the control output capacity of the actuator, the appropriate parameter k_ς is selected in (13), which is not only conducive to safe obstacle avoidance but also avoids excessive control output. To satisfy the needs of collision avoidance and formation, the inequality should be satisfied that $\|\boldsymbol{l}_i\| > R_\varsigma$.

Remark 4. The term $\boldsymbol{\varsigma}_i$ ensures that the distance between the formation mass points is always maintained at $\|\boldsymbol{\xi}_{j,1}^d - \boldsymbol{\xi}_{i,1}^d\| \geq 0$, and the term $\boldsymbol{\varsigma}_{i,k}$ ensures that the formation has a certain safety distance $\|\boldsymbol{\xi}_{i,1}^d - \boldsymbol{O}_k\| \geq R_k$ from the obstacle.

Remark 5. In a certain field of the final formation, the APF terms $\boldsymbol{\varsigma}_i$ and $\boldsymbol{\varsigma}_{i,k}$ in (10) can be eliminated. From (9) and (10), a linear system is obtained as

$$\ddot{\boldsymbol{\xi}}_{i,1}^d + c_2\dot{\boldsymbol{\xi}}_{i,1}^d + c_1\boldsymbol{\xi}_{i,1}^d = c_2\dot{\boldsymbol{\xi}}_{i,1}^r + c_1\boldsymbol{\xi}_{i,1}^r \tag{17}$$

The fewer agent operations can be used to ensure the system stability by choosing a smaller c_1 and a larger c_2.

4 | CONTROLLER DESIGN

The composite learning adaptive control with the predefined output performance and finite-time convergence is designed, the output $\boldsymbol{y}_i$ of the agent will track the reference trajectory $\boldsymbol{\xi}_{i,1}^d$ with the desired accuracy in a finite time.

Step 1: Define the tracking error $\boldsymbol{e}_{i,1}$ and the transformed error $\boldsymbol{z}_{i,1}$ as

$$\boldsymbol{e}_{i,1} = \boldsymbol{\xi}_{i,1} - \boldsymbol{\xi}_{i,1}^d \tag{18}$$

$$\boldsymbol{z}_{i,1} = \frac{1}{2}\ln\frac{1 + \boldsymbol{M}_{i,1}^{-1}(t)\boldsymbol{e}_{i,1}}{1 - \boldsymbol{M}_{i,1}^{-1}(t)\boldsymbol{e}_{i,1}} \tag{19}$$

where $\boldsymbol{M}_{i,1}(t) = \text{diag}\{\left[m_{1_{i,1}}(t), \ldots, m_{n_{i,1}}(t)\right]^T\}$ is the predefined function.

From (1), (18), and (19), $\dot{\boldsymbol{z}}_{i,1}$ is obtained as

$$\begin{aligned}\dot{\boldsymbol{z}}_{i,1} &= \frac{\partial\left(\boldsymbol{z}_{i,1}\right)}{\partial\left(\boldsymbol{M}_{i,1}^{-1}(t)\boldsymbol{e}_{i,1}\right)} \cdot \boldsymbol{M}_{i,1}^{-1}(t)\left[\dot{\boldsymbol{e}}_{i,1} - \boldsymbol{M}_{i,1}^{-1}(t)\dot{\boldsymbol{M}}_{i,1}(t)\boldsymbol{e}_{i,1}\right] \\ &= \left[\boldsymbol{M}_{i,1}^2(t) - \boldsymbol{e}_{i,1}^T\boldsymbol{e}_{i,1}\right]^{-1}\boldsymbol{M}_{i,1}(t)\left[\boldsymbol{g}_{i,1}\boldsymbol{\xi}_{i,2} - \boldsymbol{\xi}_{i,2}^d - \boldsymbol{M}_{i,1}^{-1}(t)\dot{\boldsymbol{M}}_{i,1}(t)\boldsymbol{e}_{i,1}\right]\end{aligned} \tag{20}$$

The virtual control $\boldsymbol{\xi}_{i,2}^c$ is designed as

$$\boldsymbol{\xi}_{i,2}^c = \boldsymbol{g}_{i,1}^{-1}\left[\boldsymbol{\xi}_{i,2}^d + \boldsymbol{M}_{i,1}^{-1}(t)\dot{\boldsymbol{M}}_{i,1}(t)\boldsymbol{e}_{i,1} - \hbar_{i,1}^{-1}\left(-\boldsymbol{k}_{i,1}\boldsymbol{z}_{i,1} - \boldsymbol{\kappa}_{ci,1}\boldsymbol{z}_{i,1}^{\kappa_r}\right)\right] \tag{21}$$

$$\hbar_{i,1} = \left[\boldsymbol{M}_{i,1}^2(t) - \boldsymbol{e}_{i,1}^T\boldsymbol{e}_{i,1}\right]^{-1}\boldsymbol{M}_{i,1}(t) \tag{22}$$

where $0 < \kappa_r < 1$ is positive parameter, $\boldsymbol{k}_{i,1} \in \mathfrak{R}^{n\times n}$, $\boldsymbol{k}_{i,1} = \boldsymbol{k}_{i,1}^T > 0$, $\boldsymbol{\kappa}_{ci,1} \in \mathfrak{R}^{n\times n}$, and $\boldsymbol{\kappa}_{ci,1} = \boldsymbol{\kappa}_{ci,1}^T > 0$ are the design matrices.

The new variable $\boldsymbol{\xi}_{i,2}^e$ is obtained by the first-order Levant differentiator as

$$\begin{cases}\dot{\boldsymbol{\xi}}_{i,2}^e = \boldsymbol{\xi}_{i,2}^f \\ \boldsymbol{\xi}_{i,2}^f = -\boldsymbol{\kappa}_{1i}\|\boldsymbol{\xi}_{i,2}^e - \boldsymbol{\xi}_{i,2}^c\|^{\frac{1}{2}}\tanh\left(\boldsymbol{\xi}_{i,2}^e - \boldsymbol{\xi}_{i,2}^c\right) + \boldsymbol{\xi}_{i,2}^g \\ \dot{\boldsymbol{\xi}}_{i,2}^g = -\boldsymbol{\kappa}_{2i}\tanh\left(\boldsymbol{\xi}_{i,2}^g - \boldsymbol{\xi}_{i,2}^f\right)\end{cases} \tag{23}$$

where $\boldsymbol{\kappa}_{1i} \in \mathfrak{R}^{n\times n}$, $\boldsymbol{\kappa}_{1i} = \boldsymbol{\kappa}_{1i}^T > 0$, $\boldsymbol{\kappa}_{2i} \in \mathfrak{R}^{n\times n}$, and $\boldsymbol{\kappa}_{2i} = \boldsymbol{\kappa}_{2i}^T > 0$ are the design matrices.

Define $\boldsymbol{e}_{i,2} = \boldsymbol{\xi}_{i,2} - \boldsymbol{\xi}_{i,2}^{c}$. The derivative of $\boldsymbol{z}_{i,1}$ is calculated as

$$\dot{\boldsymbol{z}}_{i,1} = -\boldsymbol{k}_{i,1}\boldsymbol{z}_{i,1} - \boldsymbol{\kappa}_{ci,1}\boldsymbol{z}_{i,1}^{\kappa_r} + \hbar_{i,1}\boldsymbol{g}_{i,1}\boldsymbol{e}_{i,2} \tag{24}$$

Step 2: From (1), (6), and (23) $\dot{\boldsymbol{e}}_{i,2}$ is obtained as

$$\dot{\boldsymbol{e}}_{i,2} = \boldsymbol{\sigma}_i^{*T}\boldsymbol{\phi}(\bar{\boldsymbol{\xi}}_{i,2}) + \boldsymbol{\varepsilon}_i + \boldsymbol{g}_{i,2}\boldsymbol{\mu}_i - \dot{\boldsymbol{\xi}}_{i,2}^{c} \tag{25}$$

The control input $\boldsymbol{\mu}_i$ is designed as

$$\boldsymbol{\mu}_i = \boldsymbol{g}_{i,2}^{-1}\left[-\hat{\boldsymbol{\sigma}}_i^{T}\boldsymbol{\phi}(\bar{\boldsymbol{\xi}}_{i,2}) + \dot{\boldsymbol{\xi}}_{i,2}^{e} - \hbar_{i,1}\boldsymbol{g}_{i,1}\boldsymbol{z}_{i,1} - \boldsymbol{k}_{i,2}\boldsymbol{e}_{i,2} - \boldsymbol{\kappa}_{ci,2}\boldsymbol{e}_{i,2}^{\kappa_r}\right] \tag{26}$$

where $\hat{\boldsymbol{\sigma}}_i$ is the estimate of the optimal neural weights $\boldsymbol{\sigma}_i^{*}$, $\boldsymbol{k}_{i,2} \in \mathfrak{R}^{n\times n}$, $\boldsymbol{k}_{i,2} = \boldsymbol{k}_{i,2}^{T} > 0$, $\boldsymbol{\kappa}_{ci,2} \in \mathfrak{R}^{n\times n}$, and $\boldsymbol{\kappa}_{ci,2} = \boldsymbol{\kappa}_{ci,2}^{T} > 0$ are the design matrices.

The derivative of $\boldsymbol{e}_{i,2}$ is calculated as

$$\dot{\boldsymbol{e}}_{i,2} = -\boldsymbol{k}_{i,2}\boldsymbol{e}_{i,2} - \hbar_{i,1}\boldsymbol{g}_{i,1}\boldsymbol{z}_{i,1} - \boldsymbol{\kappa}_{ci,2}\boldsymbol{e}_{i,2}^{\kappa_r} + \tilde{\boldsymbol{\sigma}}_i^{T}\boldsymbol{\phi}(\bar{\boldsymbol{\xi}}_{i,2}) + \boldsymbol{\varepsilon}_i + \left(\dot{\boldsymbol{\xi}}_{i,2}^{e} - \dot{\boldsymbol{\xi}}_{i,2}^{c}\right) \tag{27}$$

where $\tilde{\boldsymbol{\sigma}}_i^{T} = \boldsymbol{\sigma}_i^{*T} - \hat{\boldsymbol{\sigma}}_i^{T}$.

The prediction error $\boldsymbol{\chi}_{i,2}$ is obtained as

$$\boldsymbol{\chi}_{i,2} = \boldsymbol{\xi}_{i,2} - \hat{\boldsymbol{\xi}}_{i,2} \tag{28}$$

where the SPEM is constructed as

$$\dot{\hat{\boldsymbol{\xi}}}_{i,2} = \hat{\boldsymbol{\sigma}}_i^{T}\boldsymbol{\phi}(\bar{\boldsymbol{\xi}}_{i,2}) + \boldsymbol{g}_{i,2}\boldsymbol{\mu}_i + \boldsymbol{k}_{i,3}\boldsymbol{\chi}_{i,2} + \boldsymbol{\kappa}_{ci,3}\boldsymbol{\lambda}_{ci}^{\kappa_r}\boldsymbol{\chi}_{i,2}^{\kappa_r} \tag{29}$$

with the design matrices $\boldsymbol{k}_{i,3} \in \mathfrak{R}^{n\times n}$, $\boldsymbol{k}_{i,3} = \boldsymbol{k}_{i,3}^{T} > 0$, $\lambda_{ci} \in \mathfrak{R}^{n\times n}$, $\lambda_{ci} = \lambda_{ci}^{T} > 0$, $\boldsymbol{\kappa}_{ci,3} \in \mathfrak{R}^{n\times n}$, and $\boldsymbol{\kappa}_{ci,3} = \boldsymbol{\kappa}_{ci,3}^{T} > 0$.

The adaptive update law of $\hat{\boldsymbol{\sigma}}_i$ is proposed as

$$\dot{\hat{\boldsymbol{\sigma}}}_i = \lambda_i\left[\boldsymbol{\phi}(\bar{\boldsymbol{\xi}}_{i,2})\left(\boldsymbol{e}_{i,2} + \lambda_{ci}\boldsymbol{\chi}_{i,2}\right)^{T} - \boldsymbol{k}_{i,4}\hat{\boldsymbol{\sigma}}_i\right] \tag{30}$$

where $\lambda_i \in \mathfrak{R}^{l_{hi}\times l_{hi}}$, $\lambda_i = \lambda_i^{T} > 0$, $\boldsymbol{k}_{i,4} \in \mathfrak{R}^{l_{hi}\times l_{hi}}$, and are the design matrices.

From (1), (28), and (29), the derivative of $\boldsymbol{\chi}_{i,2}$ is rewritten as

$$\dot{\boldsymbol{\chi}}_{i,2} = \tilde{\boldsymbol{\sigma}}_i^{T}\boldsymbol{\phi}(\bar{\boldsymbol{\xi}}_{i,2}) + \boldsymbol{\varepsilon}_i - \boldsymbol{k}_{i,3}\boldsymbol{\chi}_{i,2} - \boldsymbol{\kappa}_{ci,3}\boldsymbol{\lambda}_{ci}^{\kappa_r}\boldsymbol{\chi}_{i,2}^{\kappa_r} \tag{31}$$

Remark 6. According to Lemma 1, the term $-\boldsymbol{\kappa}_{ci,1}\boldsymbol{z}_{i,1}^{\kappa_r}$ in (21), the term $-\boldsymbol{\kappa}_{ci,2}\boldsymbol{e}_{i,2}^{\kappa_r}$ in (26), and the term $\boldsymbol{\kappa}_{ci,3}\boldsymbol{\lambda}_{ci}^{\kappa_r}\boldsymbol{\chi}_{i,2}^{\kappa_r}$ in (29) ensure $\boldsymbol{z}_{i,1}$, $\boldsymbol{e}_{i,2}$, and $\boldsymbol{\chi}_{i,2}$ to be convergence in a finite time.

Remark 7. The predefined function $m_{j_{i,1}}(t)$ in (19) is chosen as $m_{j_{i,1}}(t) = \kappa_{b_{ji}}\exp\left(-\kappa_{l_{ji}}\right) + \kappa_{\varsigma_{ji}}$, where $\kappa_{b_{ji}} > 0$, $\kappa_{l_{ji}} > 0$, $\kappa_{\varsigma_{ji}} > 0$ are the predefined parameters, and $j = 1, \ldots, n$.

Remark 8. [31] If the differentiator input $\boldsymbol{\xi}_{i,2}^{c}$ without the input noise, the equalities exist $\boldsymbol{\xi}_{i,2}^{e} = \boldsymbol{\xi}_{i,2}^{c}$ and $\boldsymbol{\xi}_{i,2}^{f} = \dot{\boldsymbol{\xi}}_{i,2}^{c}$. If the differentiator input satisfy $\|\boldsymbol{\xi}_{i,2}^{cf} - \boldsymbol{\xi}_{i,2}^{c}\| \le \varrho_0$ with the input noise, the filter signals are finite-time stable with $\|\boldsymbol{\xi}_{i,2}^{e} - \boldsymbol{\xi}_{i,2}^{c}\| \le \kappa_{\varrho_{1i}}\varrho_0$ and $\|\boldsymbol{\xi}_{i,2}^{f} - \dot{\boldsymbol{\xi}}_{i,2}^{c}\| = \|\dot{\boldsymbol{\xi}}_{i,2}^{e} - \dot{\boldsymbol{\xi}}_{i,2}^{c}\| \le \kappa_{\varrho_{2i}}\varrho_0^{\frac{1}{2}}$, where $\boldsymbol{\xi}_{i,2}^{cf}$ is the virtual control with input noise, $\varrho_0 > 0$, $\kappa_{\varrho_{1i}} > 0$, and $\kappa_{\varrho_{2i}} > 0$ are the constants related to filter parameters $\boldsymbol{\kappa}_{1i}$ and $\boldsymbol{\kappa}_{2i}$. Furthermore, the hyperbolic function $\tanh(\cdot)$ can reduce the chatter problem of the design.

5 | SYSTEM STABILITY

Theorem 1. *If the virtual control (21), the control input (26) and the adaptive law (30) are designed for the uncertain MAS (1), the signals $\boldsymbol{z}_{i,1}$, $\boldsymbol{e}_{i,2}$, $\tilde{\boldsymbol{\sigma}}_i$, and $\boldsymbol{\chi}_{i,2}$ in (32) are UUB, the tracking error $\boldsymbol{e}_{i,1}$ is finite-time stable and the system output $\boldsymbol{\xi}_{i,1}$ is constrained.*

Proof. Select the Lyapunov function as follow

$$V_i = \frac{1}{2}\boldsymbol{z}_{i,1}^T\boldsymbol{z}_{i,1} + \frac{1}{2}\boldsymbol{e}_{i,2}^T\boldsymbol{e}_{i,2} + \frac{1}{2}\mathrm{tr}\{\tilde{\boldsymbol{\sigma}}_i^T\lambda_i^{-1}\tilde{\boldsymbol{\sigma}}_i\} + \frac{1}{2}\boldsymbol{\chi}_{i,2}^T\lambda_{ci}\boldsymbol{\chi}_{i,2} \tag{32}$$

From (24), (27), (30), and (31), the derivative of V_i is calculated as

$$\begin{aligned}\dot{V}_i &= -\boldsymbol{z}_{i,1}^T\boldsymbol{k}_{i,1}\boldsymbol{z}_{i,1} - \boldsymbol{e}_{i,2}^T\boldsymbol{k}_{i,2}\boldsymbol{e}_{i,2} + \mathrm{tr}\{\tilde{\boldsymbol{\sigma}}_i^T\boldsymbol{k}_{i,4}\hat{\boldsymbol{\sigma}}_i\} - \boldsymbol{\chi}_{i,2}^T\lambda_{ci}\boldsymbol{k}_{i,3}\boldsymbol{\chi}_{i,2} + \boldsymbol{e}_{i,2}^T\left(\dot{\boldsymbol{\xi}}_{i,2}^e - \dot{\boldsymbol{\xi}}_{i,2}^c\right)\\ &\quad - \boldsymbol{z}_{i,1}^T\boldsymbol{\kappa}_{ci,1}\boldsymbol{z}_{i,1}^{\kappa_r} - \boldsymbol{e}_{i,2}^T\boldsymbol{\kappa}_{ci,2}\boldsymbol{e}_{i,2}^{\kappa_r} - \boldsymbol{\chi}_{i,2}^T\lambda_{ci}\boldsymbol{\kappa}_{ci,3}\lambda_{ci}^{\kappa_r}\boldsymbol{\chi}_{i,2}^{\kappa_r} + \boldsymbol{e}_{i,2}^T\boldsymbol{\varepsilon}_i + \boldsymbol{\chi}_{i,2}^T\lambda_{ci}\boldsymbol{\varepsilon}_i\\ &\le -k_{1i_0}\boldsymbol{z}_{i,1}^T\boldsymbol{z}_{i,1} - k_{2i_0}\boldsymbol{e}_{i,2}^T\boldsymbol{e}_{i,2} - k_{4i_0}\mathrm{tr}\{\tilde{\boldsymbol{\sigma}}_i^T\tilde{\boldsymbol{\sigma}}_i\} - k_{3i_0}\boldsymbol{\chi}_{i,2}^T\lambda_{ci}\boldsymbol{\chi}_{i,2} + k_{4i_1}\mathrm{tr}\{\tilde{\boldsymbol{\sigma}}_i^T\boldsymbol{\sigma}_i^*\}\\ &\quad - \kappa_{c1i_0}\boldsymbol{z}_{i,1}^{1+\kappa_r} - \kappa_{c2i_0}\boldsymbol{e}_{i,2}^{1+\kappa_r} - \kappa_{c3i_0}\lambda_{ci}^{1+\kappa_r}\boldsymbol{\chi}_{i,2}^{1+\kappa_r} + \boldsymbol{e}_{i,2}^T\left(\dot{\boldsymbol{\xi}}_{i,2}^e - \dot{\boldsymbol{\xi}}_{i,2}^c\right) + \boldsymbol{e}_{i,2}^T\boldsymbol{\varepsilon}_i + \boldsymbol{\chi}_{i,2}^T\lambda_{ci}\boldsymbol{\varepsilon}_i\end{aligned} \tag{33}$$

where $k_{ji_0} = \lambda_{\min}\left(\boldsymbol{k}_{i,j}\right)$, $k_{ji_1} = \lambda_{\max}\left(\boldsymbol{k}_{i,j}\right)$, $\kappa_{cki_0} = \lambda_{\min}\left(\boldsymbol{\kappa}_{ci,k}\right)$, $j = 1, 2, 3, 4$, $k = 1, 2, 3$, $\lambda_{\max}(\cdot)$ and $\lambda_{\min}(\cdot)$ are the maximum and the minimum eigenvalues of the matrix, respectively.

The inequalities are considered as

$$\begin{aligned}\mathrm{tr}\{\tilde{\boldsymbol{\sigma}}_i^T\boldsymbol{\sigma}_i^*\} &\le \frac{k_{4i_0}}{2k_{4i_1}}\mathrm{tr}\{\tilde{\boldsymbol{\sigma}}_i^T\tilde{\boldsymbol{\sigma}}_i\} + \frac{k_{4i_1}}{2k_{4i_0}}\mathrm{tr}\{\boldsymbol{\sigma}_i^{*\mathrm{T}}\boldsymbol{\sigma}_i^*\}\\ \boldsymbol{e}_{i,2}^T\left(\dot{\boldsymbol{\xi}}_{i,2}^e - \dot{\boldsymbol{\xi}}_{i,2}^c\right) &\le \frac{1}{4}k_{2i_0}\boldsymbol{e}_{i,2}^T\boldsymbol{e}_{i,2} + \frac{1}{k_{2i_0}}\kappa_{\varrho_{2i}}^2\varrho_0\\ \boldsymbol{e}_{i,2}^T\boldsymbol{\varepsilon}_i &\le \frac{1}{4}k_{2i_0}\boldsymbol{e}_{i,2}^T\boldsymbol{e}_{i,2} + \frac{1}{k_{2i_0}}\bar{\varepsilon}_i^2\\ \boldsymbol{\chi}_{i,2}^T\lambda_{ci}\boldsymbol{\varepsilon}_i &\le \frac{1}{2}k_{3i_0}\boldsymbol{\chi}_{i,2}^T\lambda_{ci}\boldsymbol{\chi}_{i,2} + \frac{1}{2k_{3i_0}}\lambda_{ci_1}\bar{\varepsilon}_i^2\end{aligned} \tag{34}$$

where $\lambda_{ci_1} = \lambda_{\max}(\lambda_{ci})$.

Therefore, $\dot{V}_i$ is obtained as

$$\begin{aligned}\dot{V}_i &\le -k_{1i_0}\boldsymbol{z}_{i,1}^T\boldsymbol{z}_{i,1} - \frac{1}{2}k_{2i_0}\boldsymbol{e}_{i,2}^T\boldsymbol{e}_{i,2} - \frac{1}{2}k_{4i_0}\mathrm{tr}\{\tilde{\boldsymbol{\sigma}}_i^T\tilde{\boldsymbol{\sigma}}_i\} - \frac{1}{2}k_{3i_0}\boldsymbol{\chi}_{i,2}^T\lambda_{ci}\boldsymbol{\chi}_{i,2} + \frac{k_{4i_1}^2}{2k_{4i_0}}\mathrm{tr}\{\boldsymbol{\sigma}_i^{*\mathrm{T}}\boldsymbol{\sigma}_i^*\}\\ &\quad - \kappa_{c1i_0}\boldsymbol{z}_{i,1}^{1+\kappa_r} - \kappa_{c2i_0}\boldsymbol{e}_{i,2}^{1+\kappa_r} - \kappa_{c3i_0}\lambda_{ci}^{1+\kappa_r}\boldsymbol{\chi}_{i,2}^{1+\kappa_r} + \left(\frac{1}{k_{2i_0}} + \frac{1}{2k_{3i_0}}\lambda_{ci_1}\right)\bar{\varepsilon}_i^2 + \frac{1}{k_{2i_0}}\kappa_{\varrho_{2i}}^2\varrho_0\end{aligned} \tag{35}$$

Let $\Upsilon_i = \frac{k_{4i_1}^2}{2k_{4i_0}}\mathrm{tr}\{\boldsymbol{\sigma}_i^{*\mathrm{T}}\boldsymbol{\sigma}_i^*\} + \left(\frac{1}{k_{2i_0}} + \frac{1}{2k_{3i_0}}\lambda_{ci_1}\right)\bar{\varepsilon}_i^2 + \frac{1}{k_{2i_0}}\kappa_{\varrho_{2i}}^2\varrho_0$. The derivative of V_i can be further calculated as

$$\begin{aligned}\dot{V}_i &\le -k_{1i_0}\boldsymbol{z}_{i,1}^T\boldsymbol{z}_{i,1} - \kappa_{c1i_0}\boldsymbol{z}_{i,1}^{1+\kappa_r} - \frac{1}{2}k_{2i_0}\boldsymbol{e}_{i,2}^T\boldsymbol{e}_{i,2} - \kappa_{c2i_0}\boldsymbol{e}_{i,2}^{1+\kappa_r} - \frac{1}{2}k_{3i_0}\boldsymbol{\chi}_{i,2}^T\lambda_{ci}\boldsymbol{\chi}_{i,2} - \kappa_{c3i_0}\lambda_{ci}^{1+\kappa_r}\boldsymbol{\chi}_{i,2}^{1+\kappa_r}\\ &\quad - \frac{1}{4}k_{4i_0}\mathrm{tr}\{\tilde{\boldsymbol{\sigma}}_i^T\tilde{\boldsymbol{\sigma}}_i\} - \kappa_{c4i_0}\left(\frac{1}{4}k_{4i_0}\mathrm{tr}\{\tilde{\boldsymbol{\sigma}}_i^T\tilde{\boldsymbol{\sigma}}_i\}\right)^{\frac{1+\kappa_r}{2}} + \left[\kappa_{c4i_0}\left(\frac{1}{4}k_{4i_0}\mathrm{tr}\{\tilde{\boldsymbol{\sigma}}_i^T\tilde{\boldsymbol{\sigma}}_i\}\right)^{\frac{1+\kappa_r}{2}} - \frac{1}{4}k_{4i_0}\mathrm{tr}\{\tilde{\boldsymbol{\sigma}}_i^T\tilde{\boldsymbol{\sigma}}_i\}\right] + \Upsilon_i\end{aligned} \tag{36}$$

where $\kappa_{c4i_0} > 0$ is the design parameter.

According to Lemma 2, $\dot{V}_i$ is obtained as

$$\begin{aligned}\dot{V}_i &\le -2k_{1i_0}\left(\frac{1}{2}\boldsymbol{z}_{i,1}^T\boldsymbol{z}_{i,1}\right) - 2^{\kappa_\eta}\kappa_{c1i_0}\left(\frac{1}{2}\boldsymbol{z}_{i,1}^T\boldsymbol{z}_{i,1}\right)^{\kappa_\eta} - k_{2i_0}\left(\frac{1}{2}\boldsymbol{e}_{i,2}^T\boldsymbol{e}_{i,2}\right) - 2^{\kappa_\eta}\kappa_{c2i_0}\left(\frac{1}{2}\boldsymbol{e}_{i,2}^T\boldsymbol{e}_{i,2}\right)^{\kappa_\eta}\\ &\quad - k_{3i_0}\left(\frac{1}{2}\boldsymbol{\chi}_{i,2}^T\lambda_{ci}\boldsymbol{\chi}_{i,2}\right) - 2^{\kappa_\eta}\kappa_{c3i_0}\left(\frac{1}{2}\boldsymbol{\chi}_{i,2}^T\lambda_{ci}\boldsymbol{\chi}_{i,2}\right)^{\kappa_\eta} - \left(\frac{1}{2}k_{4i_0}\lambda_{i_0}\right)^{\kappa_\eta}\kappa_{c4i_0}\left(\frac{1}{2}\mathrm{tr}\{\tilde{\boldsymbol{\sigma}}_i^T\lambda_i^{-1}\tilde{\boldsymbol{\sigma}}_i\}\right)^{\kappa_\eta}\\ &\quad - \frac{1}{2}k_{4i_0}\lambda_{i_0}\left(\frac{1}{2}\mathrm{tr}\{\tilde{\boldsymbol{\sigma}}_i^T\lambda_i^{-1}\tilde{\boldsymbol{\sigma}}_i\}\right) + \Upsilon_{i1}\end{aligned} \tag{37}$$

where $\kappa_\eta = \frac{1+\kappa_r}{2}$, $\lambda_{i_0} = \lambda_{\min}(\lambda_i)$, and $\Upsilon_{i1} = \Upsilon_i + \kappa_{c4i_0}$.

The parameters $k_{ji_0} > 0$, $\kappa_{cji_0} > 0$, and $\lambda_{i_0} > 0$ are selected, where $j = 1, 2, 3, 4$. It can be concluded that

$$\dot{V}_i \leq -k_{vi} V_i - \kappa_{vi} V_i^{\kappa_\eta} + \Upsilon_{i1} \tag{38}$$

where $k_{vi} = \min\left\{2k_{1i_0}, k_{2i_0}, k_{3i_0}, \frac{1}{2}k_{4i_0}\lambda_{i_0}\right\}$ and $\kappa_{vi} = \min\left\{2^{\kappa_\eta}\kappa_{c1i_0}, 2^{\kappa_\eta}\kappa_{c2i_0}, 2^{\kappa_\eta}\kappa_{c3i_0}, \left(\frac{1}{2}k_{4i_0}\lambda_{i_0}\right)^{\kappa_\eta}\kappa_{c4i_0}\right\}$.

The errors in the Lyapunov function (32) are finite-time stable from Lemma 1, the boundary and the setting time are calculated as

$$V_i \leq \min\left\{\frac{\Upsilon_{i1}}{\left(1-\kappa_{\theta_0}\right)k_{vi}}, \left[\frac{\Upsilon_{i1}}{\left(1-\kappa_{\theta_0}\right)\kappa_{vi}}\right]^{\frac{1}{\kappa_\eta}}\right\} \tag{39}$$

$$T_{i1} \leq \left\{t_0 + \frac{1}{\kappa_{\theta_0}k_{vi}\left(1-\kappa_\eta\right)}\ln\frac{\kappa_{\theta_0}k_{vi}V_i^{1-\kappa_\eta}(t_0)+\kappa_{vi}}{\kappa_{vi}},\ t_0 + \frac{1}{k_{vi}\left(1-\kappa_\eta\right)}\ln\frac{k_{vi}V_i^{1-\kappa_\eta}(t_0)+\kappa_{\theta_0}\kappa_{vi}}{\kappa_{\theta_0}\kappa_{vi}}\right\} \tag{40}$$

Through the analysis in (32,33,34,35,36,37,38,39,40), the transformed error $\boldsymbol{z}_{i,1}$ is bounded. Then it can be calculated that the tracking error $\boldsymbol{e}_{i,1}$ satisfies $|e_{j_{i,1}}| < m_{j_{i,1}}(t)$ and the system output of agent is constrained in the region $|\xi_{j_{i,1}}| < |\xi^d_{j_{i,1}}| + m_{j_{i,1}}(t)$, where $j = 1, \ldots, n$, $\boldsymbol{e}_{i,1} = \left[e_{1_{i,1}}, \ldots, e_{n_{i,1}}\right]$, $\boldsymbol{\xi}_{i,1} = \left[\xi_{1_{i,1}}, \ldots, \xi_{n_{i,1}}\right]$, and $\boldsymbol{\xi}^d_{i,1} = \left[\xi^d_{1_{i,1}}, \ldots, \xi^d_{n_{i,1}}\right]$.

This completes the proof. ∎

Based on the above analysis, the algorithm of the proposed controller is presented as

Algorithm 1. Control Design Algorithm

Step 1: Obtain the location information of obstacles $\boldsymbol{O}_k$ and $\boldsymbol{R}_k$, set the formation operation structure $\boldsymbol{l}_i$ and desired goals

$\boldsymbol{\xi}^r_1$ and $\boldsymbol{\xi}^r_2$.

Step 2: The input for the motion model (9) can be design as follows:

$$\boldsymbol{\tau}_i = c_1\left(\boldsymbol{\xi}^r_{i,1} - \boldsymbol{\xi}^d_{i,1}\right) + c_2\left(\boldsymbol{\xi}^r_{i,2} - \boldsymbol{\xi}^d_{i,2}\right) + \boldsymbol{\varsigma}_i + \boldsymbol{\varsigma}_{i,k}$$

Step 3: The composite learning control for system (1) can be proposed as follows:

$$\boldsymbol{\mu}_i = \boldsymbol{g}^{-1}_{i,2}\left[-\hat{\boldsymbol{\sigma}}^T_i\boldsymbol{\phi}(\bar{\boldsymbol{\xi}}_{i,2}) + \dot{\boldsymbol{\xi}}^e_{i,2} - \hbar_{i,1}\boldsymbol{g}_{i,1}\boldsymbol{z}_{i,1} - \boldsymbol{k}_{i,2}\boldsymbol{e}_{i,2} - \boldsymbol{\kappa}_{ci,2}\boldsymbol{e}^{\kappa_r}_{i,2}\right]$$

Remark 9. The transformed error $\boldsymbol{z}_{i,1}$, tracking error $\boldsymbol{e}_{i,2}$, learning error $\tilde{\boldsymbol{\sigma}}_i$, and prediction error $\boldsymbol{\chi}_{i,2}$ will converge to a small set by increasing the control parameters $\boldsymbol{k}_{i,j}$, λ_i, $\boldsymbol{\kappa}_{ci,j}$ and decreasing the parameters λ_{ci}. The convergence time T_{i1} is determined by the parameters $\boldsymbol{k}_{i,j}$, λ_i, $\boldsymbol{\kappa}_{ci,j}$, λ_{ci}, while the learning performance is affected by the parameters λ_i, λ_{ci}, and $\boldsymbol{k}_{i,4}$, where $j = 1, 2, 3, 4$.

6 | SIMULATION

In the section, ten AUVs randomly distributed on the water surface sail in a triangular formation and accurately avoid three obstacles under the designed controller. The approach in the article is marked as "CNL-FC", while the control method only introducing tracking error into neural update law is denoted as "NNL". For comparison, the method without finite time is called as "CNL".

The dynamics of the multi-AUV system[28] are described as

$$\begin{cases}\dot{\boldsymbol{\eta}}_i = \boldsymbol{R}_i(\psi_i)\,\boldsymbol{\vartheta}_i \\ \dot{\boldsymbol{\vartheta}}_i = \boldsymbol{f}_i(\boldsymbol{\vartheta}_i) + \boldsymbol{M}_i^{-1}\boldsymbol{\mu}_i\end{cases} \tag{41}$$

where $\boldsymbol{\eta}_i = [x_i, y_i, \psi_i]^T \in \mathfrak{R}^3$ are the position and the heading of the ith AUV in the earth coordinate system, $\boldsymbol{\vartheta}_i = [u_i, v_i, r_i]^T \in \mathfrak{R}^3$ are the linear velocity and yaw angular velocity of the ith AUV in the body coordinate system, $\boldsymbol{\mu}_i = [\mu_{ui}, \mu_{vi}, \mu_{ri}] \in \mathfrak{R}^3$ is the control force, $\boldsymbol{R}_i(\psi_i) = \begin{bmatrix} \cos(\psi_i) & -\sin(\psi_i) & 0 \\ \sin(\psi_i) & \cos(\psi_i) & 0 \\ 0 & 0 & 1 \end{bmatrix}$ is the coordinate transformation matrix, $\boldsymbol{f}_i(\boldsymbol{\vartheta}_i) = \boldsymbol{M}_i^{-1}\left[-\boldsymbol{C}_i(\boldsymbol{\vartheta}_i)\boldsymbol{\vartheta}_i - \boldsymbol{D}_i(\boldsymbol{\vartheta}_i)\boldsymbol{\vartheta}_i\right] = \left[f_{ui}, f_{vi}, f_{ri}\right]^T$ is the unknown dynamics uncertainty, $\boldsymbol{M}_i = \begin{bmatrix} 215 & 0 & 0 \\ 0 & 215 & 0 \\ 0 & 0 & 80 \end{bmatrix}$ is the inertial mass matrix, $\boldsymbol{C}_i(\boldsymbol{\vartheta}_i) = \begin{bmatrix} 0 & 0 & -215v_i \\ 0 & 0 & 215u_i \\ 215v_i & -215u_i & 0 \end{bmatrix}$ is the centripetal force and coriolis force matrix, and $\boldsymbol{D}_i(\boldsymbol{\vartheta}_i) = -\begin{bmatrix} 100+100|u_i| & 0 & 0 \\ 0 & 200+300|v_i| & 0 \\ 0 & 0 & 50+50|r_i| \end{bmatrix}$ is the damping force matrix, where $i = 1, \ldots, 10$.

Define the position as $\boldsymbol{q}_r = [x_r, y_r]^T \in \mathfrak{R}^2$ and the velocity as $\boldsymbol{p}_r = [u_r, v_r]^T \in \mathfrak{R}^2$. The desired virtual structure formation is formed as

$$\begin{cases} \boldsymbol{q}_{ri} = \boldsymbol{q}_r + \boldsymbol{R}(\psi_r)\boldsymbol{l}_i \\ \boldsymbol{p}_{ri} = \boldsymbol{p}_r + \dot{\boldsymbol{R}}(\psi_r)\boldsymbol{l}_i \end{cases} \tag{42}$$

where $\boldsymbol{q}_r = [t+200, 150]^T$m, $\boldsymbol{p}_r = [1, 0]^T$m/s, $\boldsymbol{R}(\psi_r) = \begin{bmatrix} \cos\psi_r & -\sin\psi_r \\ \sin\psi_r & \cos\psi_r \end{bmatrix}$, $\psi_r = 0$rad, $\boldsymbol{l}_1 = [30, 0]^T$m, $\boldsymbol{l}_2 = [10, -20]^T$m, $\boldsymbol{l}_3 = [10, 20]^T$m, $\boldsymbol{l}_4 = [-10, -40]^T$m, $\boldsymbol{l}_5 = [-10, 0]^T$m, $\boldsymbol{l}_6 = [-30, 40]^T$m, $\boldsymbol{l}_7 = [-30, -60]^T$m, $\boldsymbol{l}_8 = [-30, -30]^T$m, $\boldsymbol{l}_9 = [-30, 30]^T$m, and $\boldsymbol{l}_{10} = [-30, 60]^T$m.

The motion model of the VSP is established as

$$\begin{cases} \dot{\boldsymbol{q}}_i = \boldsymbol{p}_i \\ \dot{\boldsymbol{p}}_i = \boldsymbol{\tau}_i \end{cases} \tag{43}$$

where $\boldsymbol{q}_i = \left[x_i^d, y_i^d\right]^T \in \mathfrak{R}^2$ is the position, $\boldsymbol{p}_i = \left[u_i^d, v_i^d\right]^T \in \mathfrak{R}^2$ is the velocity, and $\boldsymbol{\tau}_i \in \mathfrak{R}^2$ is the input.

The input $\boldsymbol{\tau}_i$ is designed as

$$\boldsymbol{\tau}_i = c_1\left(\boldsymbol{q}_{ri} - \boldsymbol{q}_i\right) + c_2\left(\boldsymbol{p}_{ri} - \boldsymbol{p}_i\right) + \boldsymbol{\varsigma}_i + \boldsymbol{\varsigma}_{i,k} \tag{44}$$

where

$$\boldsymbol{\varsigma}_i = -\nabla_{\boldsymbol{q}i} V\left(\overline{\boldsymbol{q}}\right), \quad V\left(\overline{\boldsymbol{q}}\right) = \sum_{j \neq i}^{N} \varphi\left(\left\|\boldsymbol{q}_j - \boldsymbol{q}_i\right\|\right) \tag{45}$$

$$\boldsymbol{\varsigma}_{i,k} = -\nabla_{\boldsymbol{q}i} V_k\left(\overline{\boldsymbol{q}}\right), \quad V_k\left(\overline{\boldsymbol{q}}\right) = \sum_{k=1}^{N_1} \varphi\left(\left\|\boldsymbol{q}_{i,k} - \boldsymbol{q}_i\right\|\right) \tag{46}$$

$$\boldsymbol{q}_{i,k} = \boldsymbol{O}_k + R_k \frac{\left(\boldsymbol{q}_i - \boldsymbol{O}_k\right)}{\left\|\boldsymbol{q}_i - \boldsymbol{O}_k\right\|} \tag{47}$$

with $c_1 = 0.05$, $c_2 = 0.5$, $k_\varsigma = 4$, $R_\varsigma = 5$, $\boldsymbol{O}_1 = [500, 150]^T$m, $\boldsymbol{O}_2 = [300, 100]^T$m, $\boldsymbol{O}_3 = [300, 200]^T$m, $R_1 = 40$m, $R_2 = 20$m, and $R_3 = 10$m.

Define the reference command as $\boldsymbol{\eta}_i^d = \left[x_i^d, y_i^d, \psi_i^d\right]^T$, where $\psi_i^d = \arctan(\frac{v_i^d}{u_i^d})$. The transformed error is defined as

$$\boldsymbol{z}_{1i} = \frac{1}{2}\ln\frac{1 + \boldsymbol{m}_{1i}^{-1}(t)\boldsymbol{e}_{1i}}{1 - \boldsymbol{m}_{1i}^{-1}(t)\boldsymbol{e}_{1i}} \tag{48}$$

where $\boldsymbol{e}_{1i} = \left[e_{xi}, e_{yi}, e_{\psi i}\right]^T = \boldsymbol{\eta}_i - \boldsymbol{\eta}_i^d$, and $\boldsymbol{m}_{1i} = \text{diag}\{\left[10e^{-0.07t} + 1, 10e^{-0.07t} + 1, 10e^{-0.07t} + 1\right]^T\}$.

Define $\boldsymbol{e}_{2i} = \boldsymbol{\vartheta}_i - \boldsymbol{\vartheta}_i^c$. The virtual control $\boldsymbol{\vartheta}_i^c$ and the control input $\boldsymbol{\mu}_i$ are proposed as

$$\boldsymbol{\vartheta}_i^c = \boldsymbol{R}^{-1}(\psi_i)\left[\dot{\boldsymbol{\eta}}_i^d + \boldsymbol{m}_{1i}^{-1}(t)\dot{\boldsymbol{m}}_{1i}(t)\boldsymbol{e}_{1i} - \hbar_{i,1}^{-1}\left(-\boldsymbol{k}_{1i}\boldsymbol{z}_{1i} - \boldsymbol{\kappa}_{c1i}\boldsymbol{z}_{1i}^{\kappa_r}\right)\right] \tag{49}$$

$$\boldsymbol{\mu}_i = \boldsymbol{M}_i\left[-\hat{\boldsymbol{\sigma}}_i^T\boldsymbol{\phi}(\boldsymbol{\vartheta}_i) + \dot{\boldsymbol{\vartheta}}_i^e - \hbar_{i,1}\boldsymbol{R}(\psi_i)\boldsymbol{z}_{1i} - \boldsymbol{k}_{2i}\boldsymbol{e}_{2i} - \boldsymbol{\kappa}_{c2i}\boldsymbol{e}_{2i}^{\kappa_r}\right] \tag{50}$$

where the new signal $\dot{\boldsymbol{\vartheta}}_i^e$ is obtained as

$$\begin{cases} \dot{\boldsymbol{\vartheta}}_i^e = \boldsymbol{\vartheta}_i^f \\ \boldsymbol{\vartheta}_i^f = -\boldsymbol{\kappa}_{1i}\|\boldsymbol{\vartheta}_i^d - \boldsymbol{\vartheta}_i^c\|^{\frac{1}{2}}\tanh\left(\boldsymbol{\vartheta}_i^d - \boldsymbol{\vartheta}_i^c\right) + \boldsymbol{\vartheta}_i^g \\ \dot{\boldsymbol{\vartheta}}_i^g = -\boldsymbol{\kappa}_{2i}\tanh\left(\boldsymbol{\vartheta}_i^g - \boldsymbol{\vartheta}_i^f\right) \end{cases} \tag{51}$$

with $\hbar_{1i} = \left[\boldsymbol{m}_{1i}^2(t) - \boldsymbol{e}_{1i}^T\boldsymbol{e}_{1i}\right]^{-1}\boldsymbol{m}_{1i}(t)$, $\boldsymbol{k}_{1i} = 5\boldsymbol{I}_3$, $\boldsymbol{\kappa}_{c1i} = 0.5\boldsymbol{I}_3$, $\kappa_r = 0.6$, $\boldsymbol{k}_{2i} = 5\boldsymbol{I}_3$, $\boldsymbol{\kappa}_{c2i} = 0.5\boldsymbol{I}_3$, $\boldsymbol{\kappa}_{1i} = 100\boldsymbol{I}_3$, and $\boldsymbol{\kappa}_{2i} = 10^{-4}\boldsymbol{I}_3$.

The prediction error $\boldsymbol{\chi}_i$ is designed as

$$\boldsymbol{\chi}_i = \boldsymbol{\vartheta}_i - \hat{\boldsymbol{\vartheta}}_i \tag{52}$$

where the SPEM is constructed as

$$\dot{\hat{\boldsymbol{\vartheta}}}_i = \hat{\boldsymbol{\sigma}}_i^T\boldsymbol{\phi}(\boldsymbol{\vartheta}_i) + \boldsymbol{M}_i^{-1}\boldsymbol{\mu}_i + \boldsymbol{k}_{3i}\boldsymbol{\chi}_i + \boldsymbol{\kappa}_{c3i}\lambda_{\chi i}^{\kappa_r}\boldsymbol{\chi}_i^{\kappa_r} \tag{53}$$

with $\boldsymbol{\chi}_i = \left[\chi_{ui}, \chi_{vi}, \chi_{ri}\right]^T$, $\boldsymbol{k}_{3i} = 0.1\boldsymbol{I}_3$, $\lambda_{\chi i} = 200\boldsymbol{I}_3$, and $\boldsymbol{\kappa}_{c3i} = 0.1\boldsymbol{I}_3$.

The adaptive update law of $\hat{\boldsymbol{\sigma}}_i$ is proposed as

$$\dot{\hat{\boldsymbol{\sigma}}}_i = \lambda_i\left[\boldsymbol{\phi}(\boldsymbol{\vartheta}_i)\left(\boldsymbol{e}_{2i} + \lambda_{\chi i}\boldsymbol{\chi}_i\right)^T - \boldsymbol{k}_{4i}\hat{\boldsymbol{\sigma}}_i\right] \tag{54}$$

where $\iota_{hi} = 147$, $\lambda_i = 0.1\boldsymbol{I}_{147}$, and $\boldsymbol{k}_{4i} = 0.01\boldsymbol{I}_{147}$.

The simulations are presented in Figures 2,3,4,5,6,7,8,9,10,11,12,13. In Figure 2, the trajectories show that under randomly distributed initial positions, ten AUVs travel in a triangular formation and avoid three obstacle areas on the route. It is found that the formation track and the obstacle avoidance under "CNL-FC" are implemented. From the distance between AUVs and obstacles in Figure 3, it can be seen that the AUV formation is performing obstacle avoidance maneuvers within [70,170]s and [220,380]s, respectively. The minimums distance between AUV and the boundaries of the three obstacles are 42.46, 23.49, and 13.63m, respectively. Ten AUVs keep a certain safe distance from three obstacles under the action of collision avoidance potential function. The distances between the AUVs in Figure 4 display that although the AUV formation is destroyed by the interference of obstacles, the AUVs never collide.

Define the tracking performance indexes as $J_{ei}(\text{IAE}) = \int_0^T\|\boldsymbol{e}_{1i}(\tau)\|\mathrm{d}\tau$ and $J_{ei}(\text{ITAE}) = \int_0^T\tau\|\boldsymbol{e}_{1i}(\tau)\|\mathrm{d}\tau$. The tracking curves of system output $\boldsymbol{\eta}_1$ are shown in Figure 5, it is founded that the control ability under "CNL-FC" method seems relatively strong, and the position x_1, y_1 and the heading ψ_1 track the reference signal $\boldsymbol{\eta}_1^d$ with faster convergence and higher accuracy. In Figure 6, the tracking error signals $\boldsymbol{e}_{11}$ are restricted by $\boldsymbol{m}_{11}$ through the use of predefined performance control. The errors $\boldsymbol{e}_{11}$ under "NNL" method fluctuate in the interval $[-0.5, 0.12]$ m, $[-0.3, 0.1]$ m, $[-0.4, 0.15]$ rad, while $\boldsymbol{e}_{11}$ under "CNL" method fluctuate in the interval $[-0.13, 0.09]$ m, $[-0.04, 0.065]$ m, $[-0.07, 0.045]$ rad. For "CNL-FC" method, the amplitudes of $\boldsymbol{e}_{11}$ are smaller, and the values of $\boldsymbol{e}_{11}$ converge near zero in 4s. The similar results are manifested in Figure 7, the response curves of the tracking performance indexes demonstrate that the system energy is drastically reduced under the proposed controller. The system state $\boldsymbol{\vartheta}_1$ and the control signal $\boldsymbol{\mu}_1$ are displayed in Figures 8 and 9, respectively.

Define the approximated error as $\boldsymbol{e}_{fi} = \boldsymbol{f}_i(\boldsymbol{\vartheta}_i) - \hat{\boldsymbol{\sigma}}_i^T\boldsymbol{\phi}(\boldsymbol{\vartheta}_i)$. Define the learning performance indexes as $J_{fi}(\text{IAE}) = \int_0^T\|\boldsymbol{e}_{fi}(\tau)\|\mathrm{d}\tau$ and $J_{fi}(\text{ITAE}) = \int_0^T\tau\|\boldsymbol{e}_{fi}(\tau)\|\mathrm{d}\tau$. The estimate trajectories in Figure 10 depict that the dynamics uncertainties $\boldsymbol{f}_1(\boldsymbol{\vartheta}_1)$ are approximated accurately under the proposed controller. The response of learning performance indexes are displayed in Figure 11, the mean values under "NNL" method are 632.2 and 55,210, while the mean values under "CNL-FC" method are 4.68 and 666.1. Figure 12 shows that the trajectories of the prediction error $\boldsymbol{\chi}_1$ is bounded in a finite

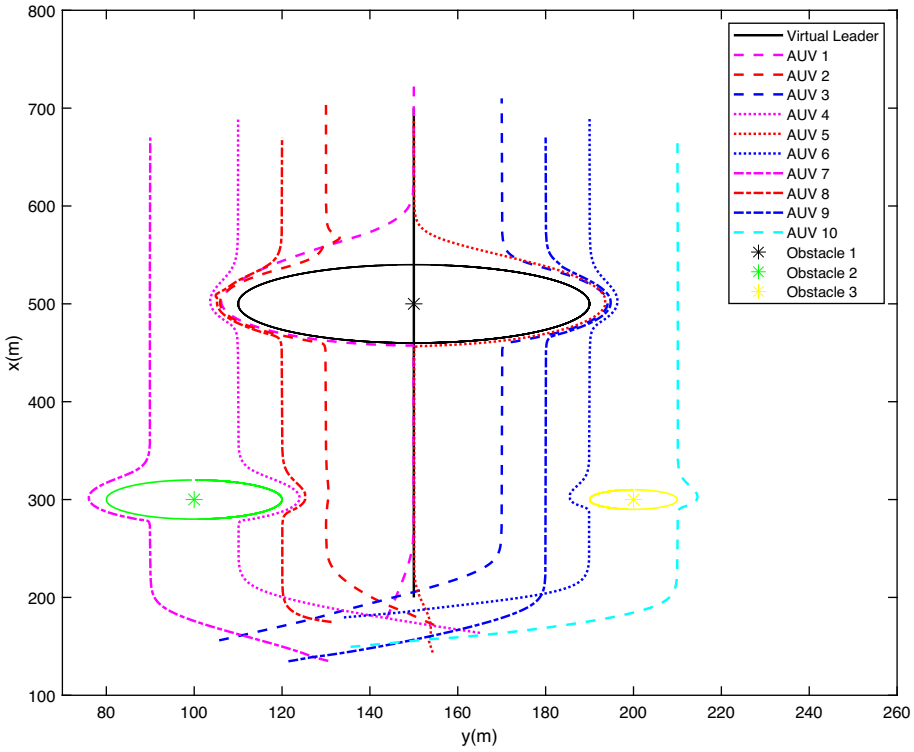

FIGURE 2 Trajectories of ten AUVs [Colour figure can be viewed at wileyonlinelibrary.com]

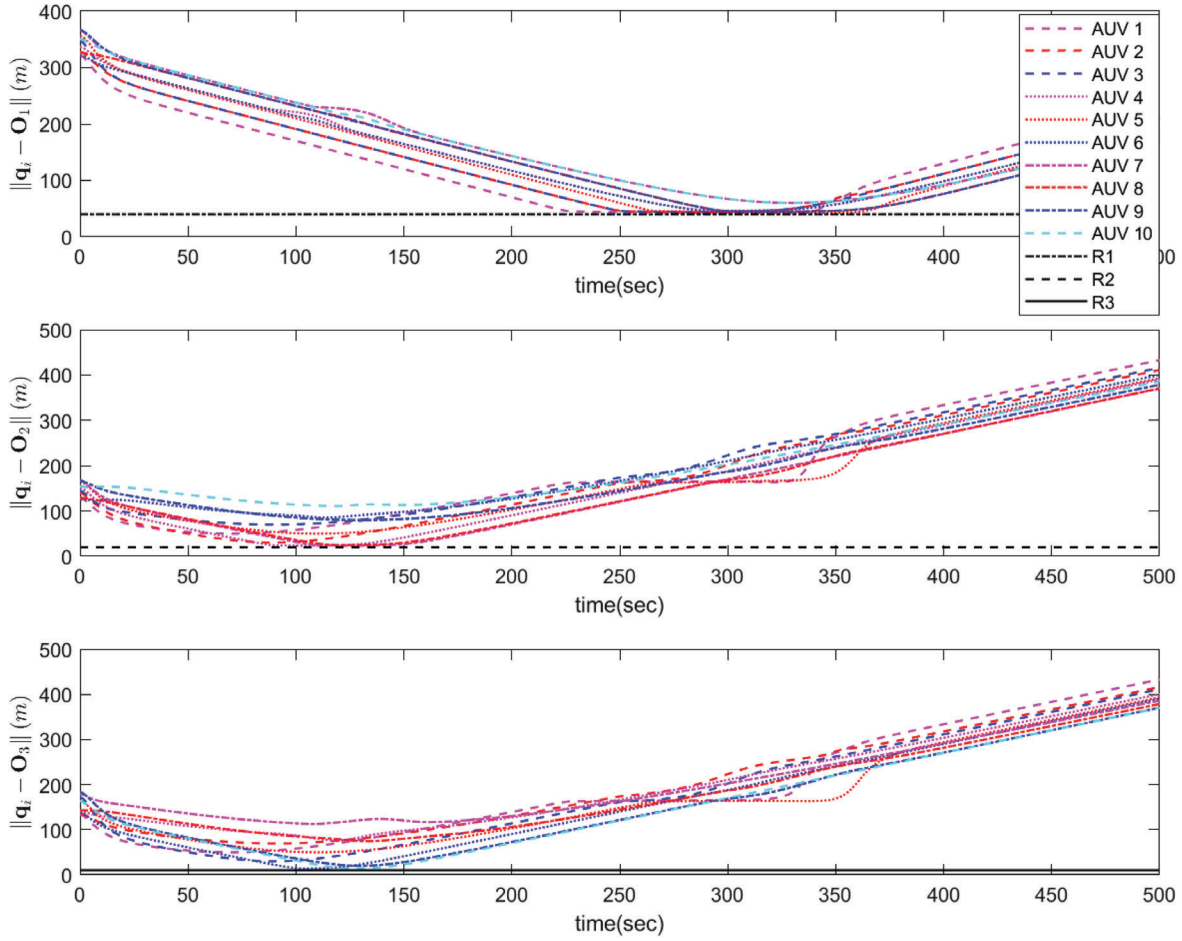

FIGURE 3 Distance between AUV and Obstacle $\|\boldsymbol{q}_i - \boldsymbol{O}_k\|$. [Colour figure can be viewed at wileyonlinelibrary.com]

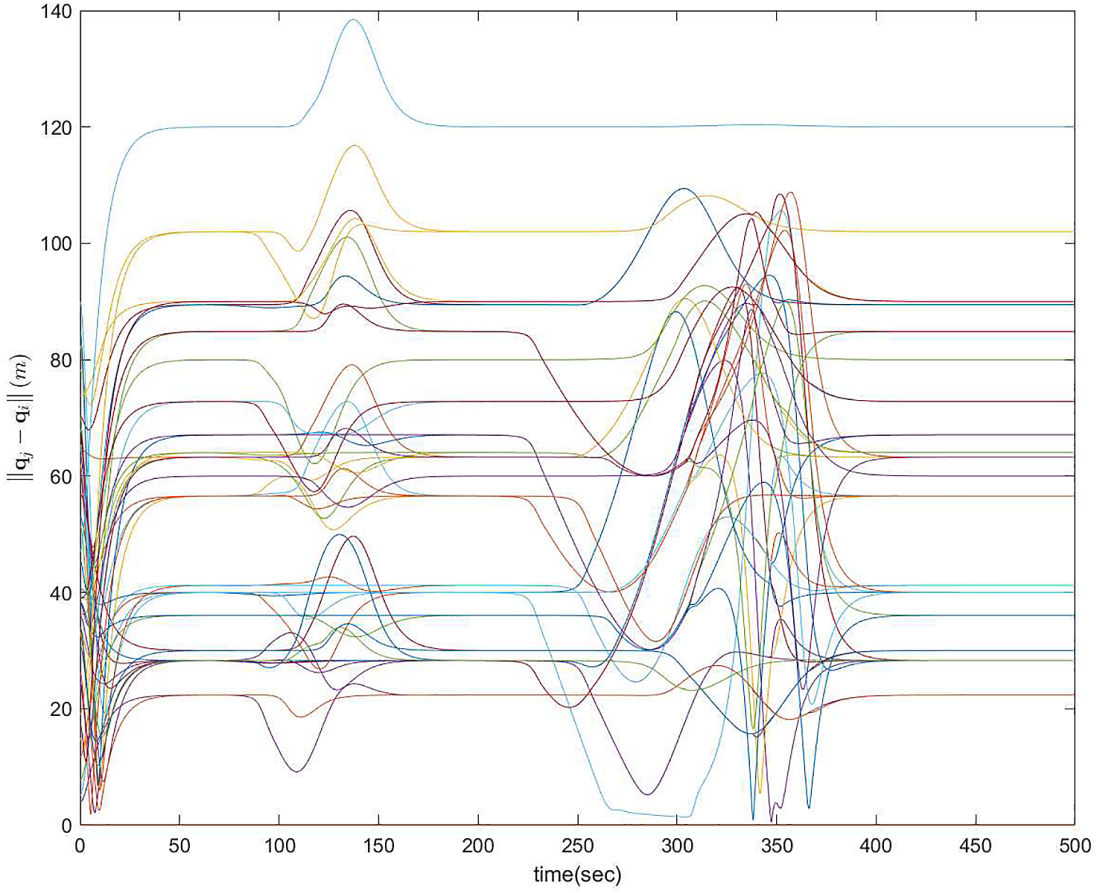

FIGURE 4 Distance between AUVs $\|\boldsymbol{q}_j - \boldsymbol{q}_i\|$. [Colour figure can be viewed at wileyonlinelibrary.com]

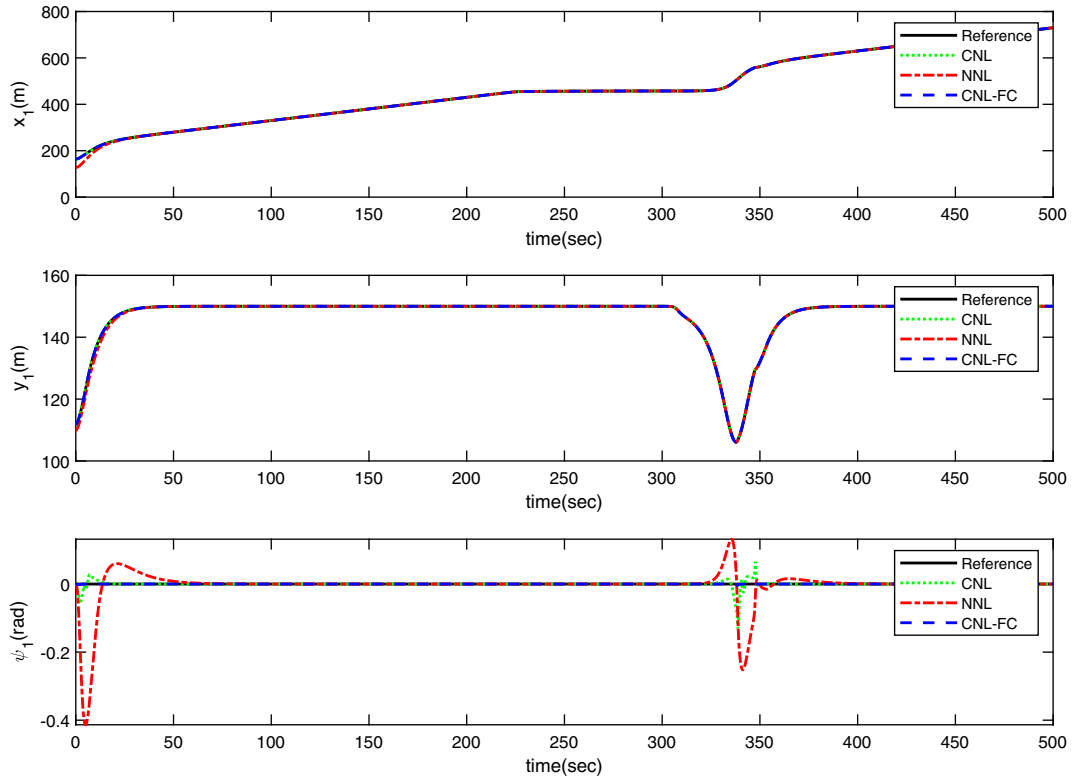

FIGURE 5 System output tracking under three method [Colour figure can be viewed at wileyonlinelibrary.com]

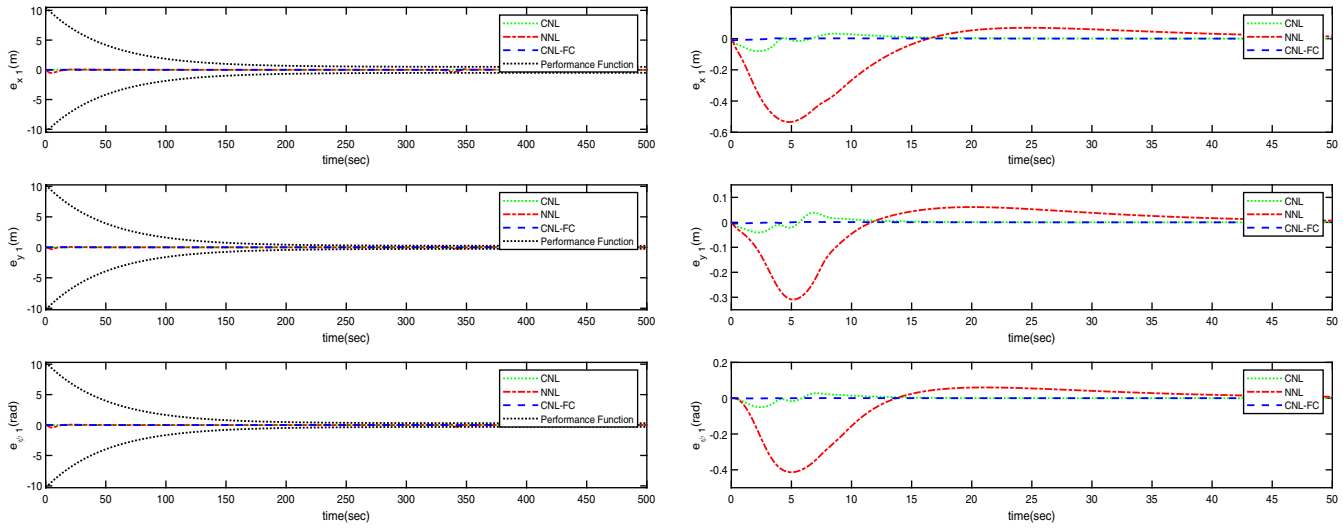

FIGURE 6 Tracking error $\boldsymbol{e}_{11}$ under three method and $\boldsymbol{e}_{11}$ in $[0, 50]$ s [Colour figure can be viewed at wileyonlinelibrary.com]

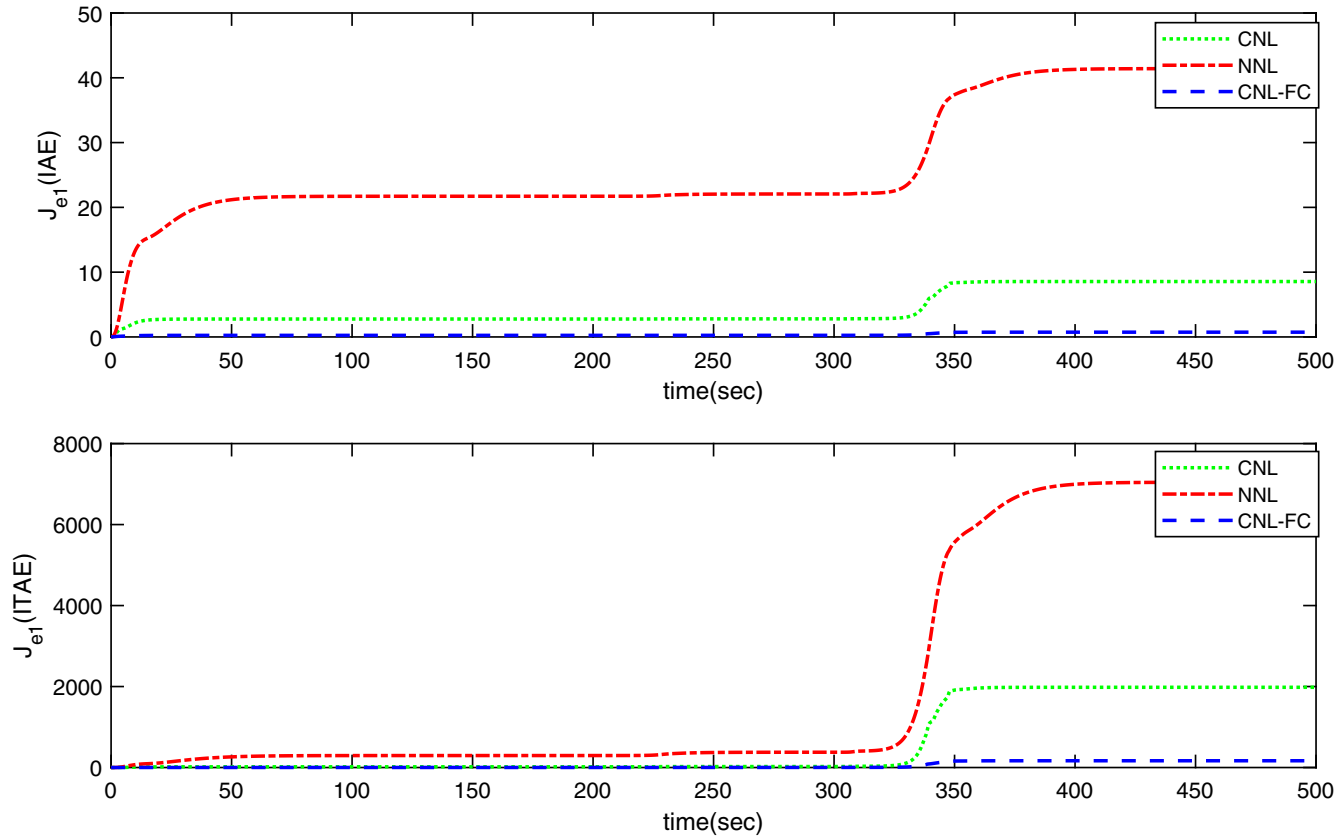

FIGURE 7 Tracking performance indexec J_{e1} (IAE) and J_{e1} (ITAE) under three method [Colour figure can be viewed at wileyonlinelibrary.com]

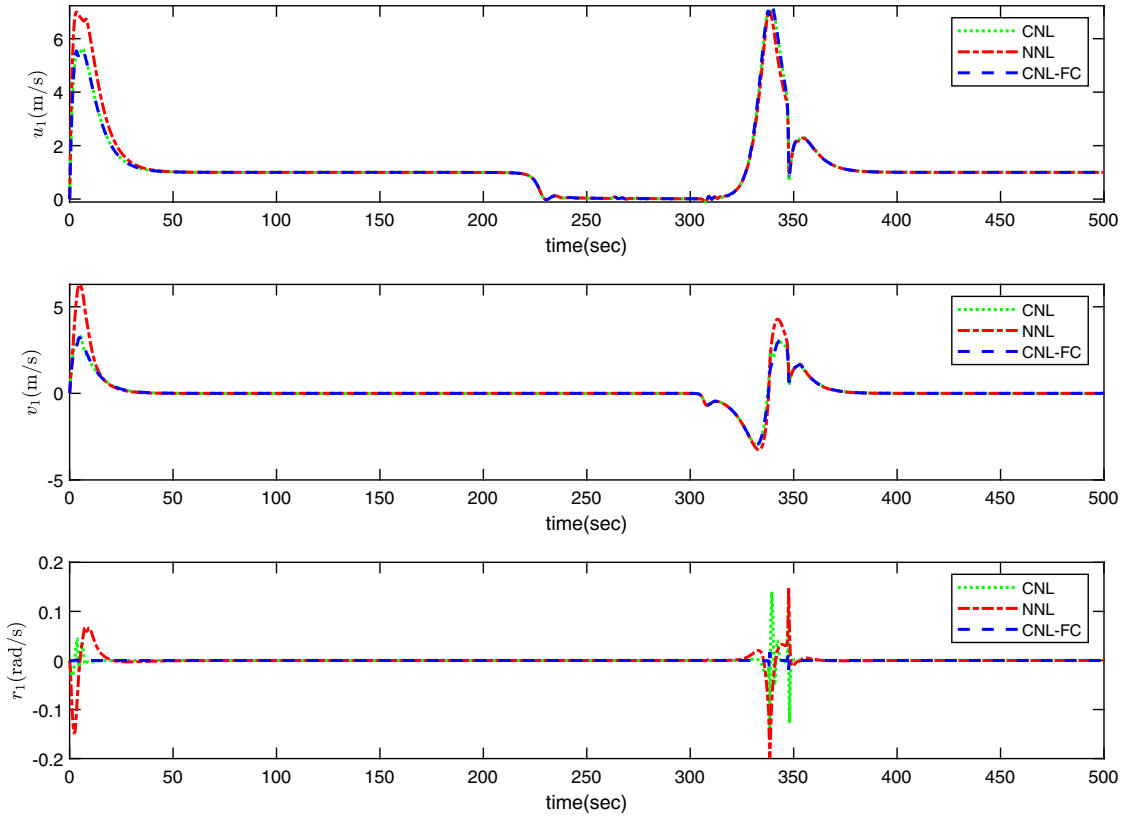

FIGURE 8 System control state ϑ_1 under three method [Colour figure can be viewed at wileyonlinelibrary.com]

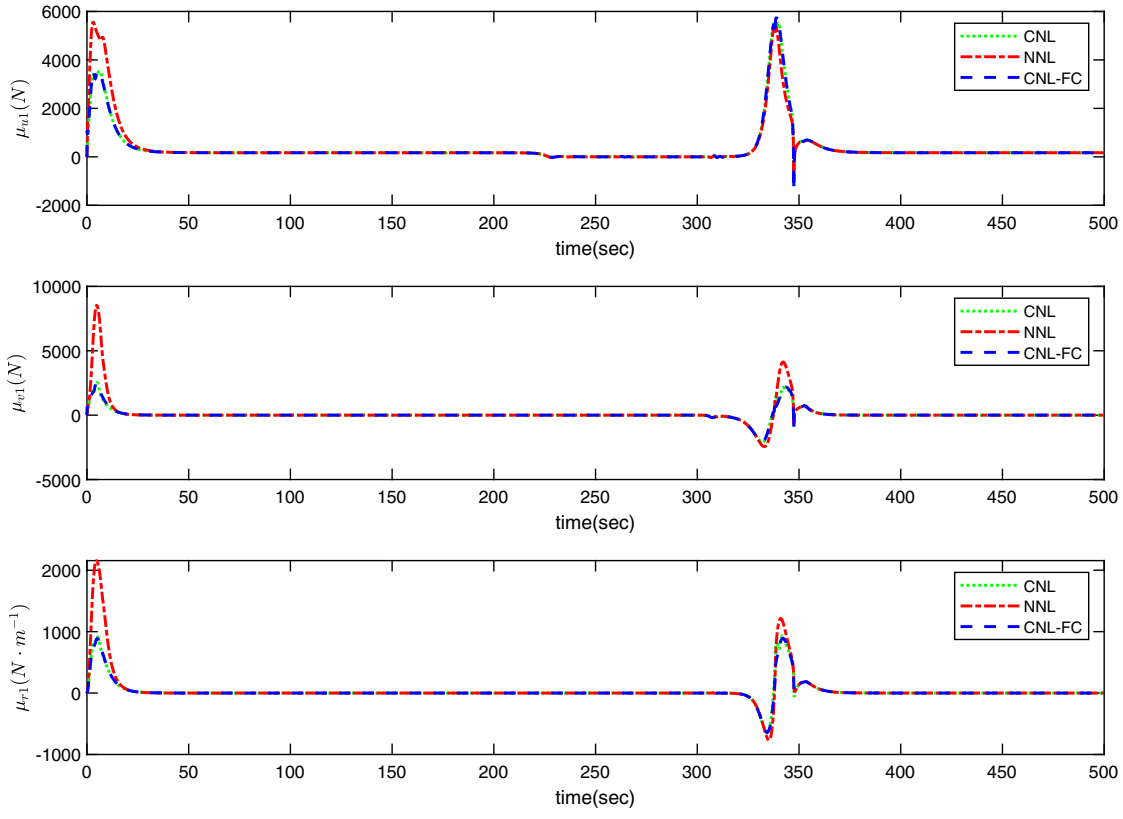

FIGURE 9 System control input $\boldsymbol{\mu}_1$ under three method [Colour figure can be viewed at wileyonlinelibrary.com]

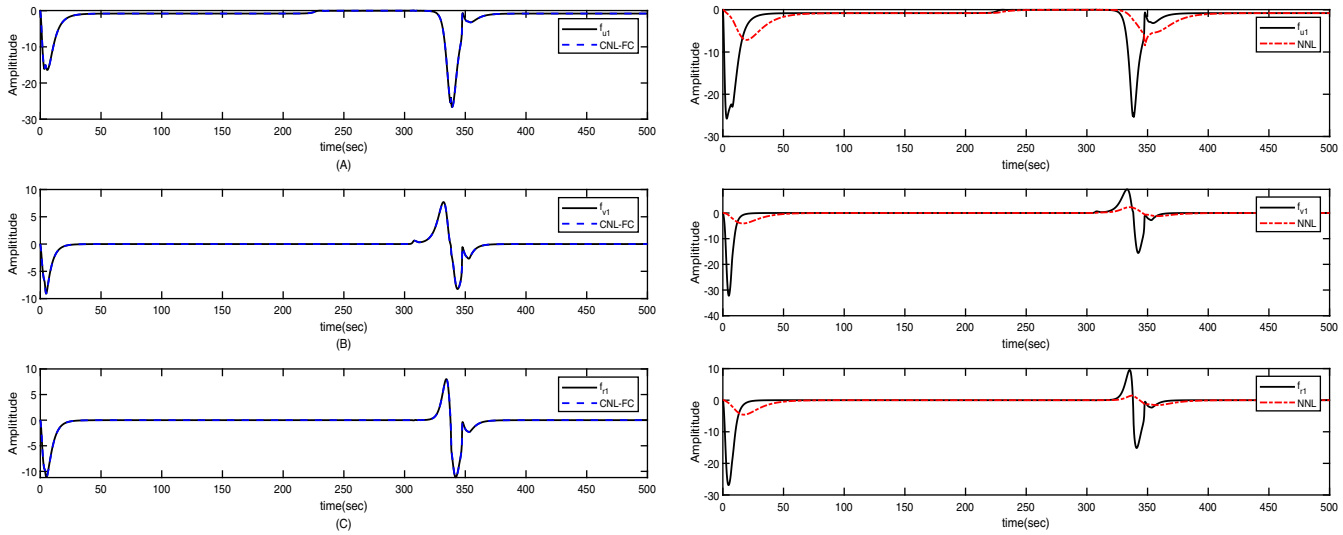

FIGURE 10 Estimate of $\boldsymbol{f}_1(\boldsymbol{\vartheta}_1)$ under "CNL-FC" method and "NNL" method [Colour figure can be viewed at wileyonlinelibrary.com]

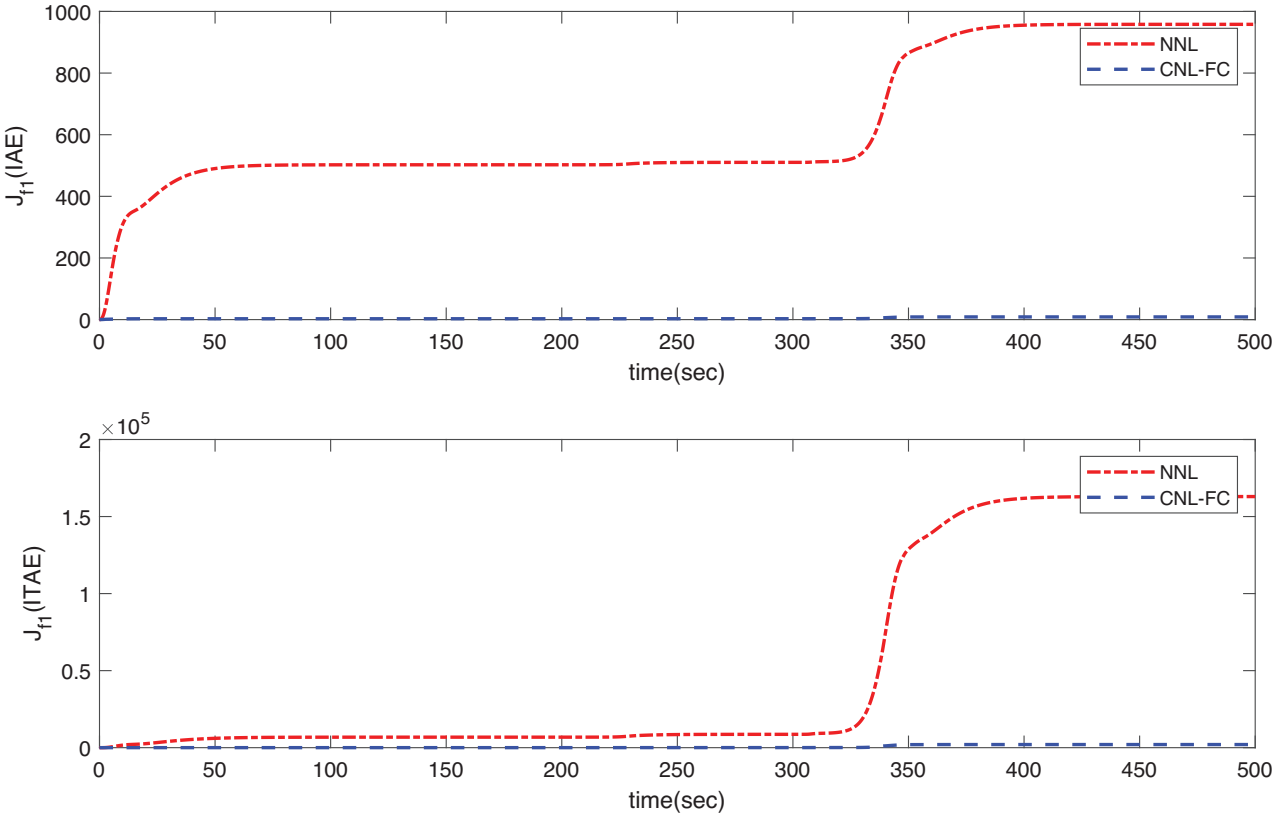

FIGURE 11 Learning performance indexec J_{f1} (IAE) and J_{f1} (ITAE) under "CNL-FC" method and "NNL" method [Colour figure can be viewed at wileyonlinelibrary.com]

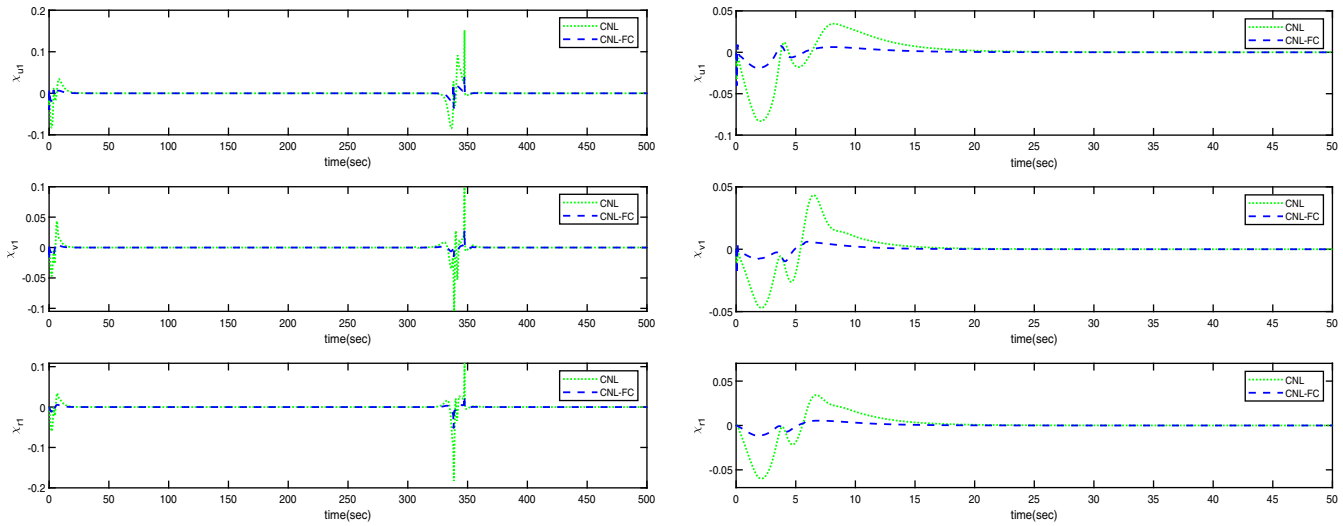

FIGURE 12 Trajectories of prediction error χ_1 under "CNL-FC" method and "CNL" method and χ_1 in $[0, 50]$ s [Colour figure can be viewed at wileyonlinelibrary.com]

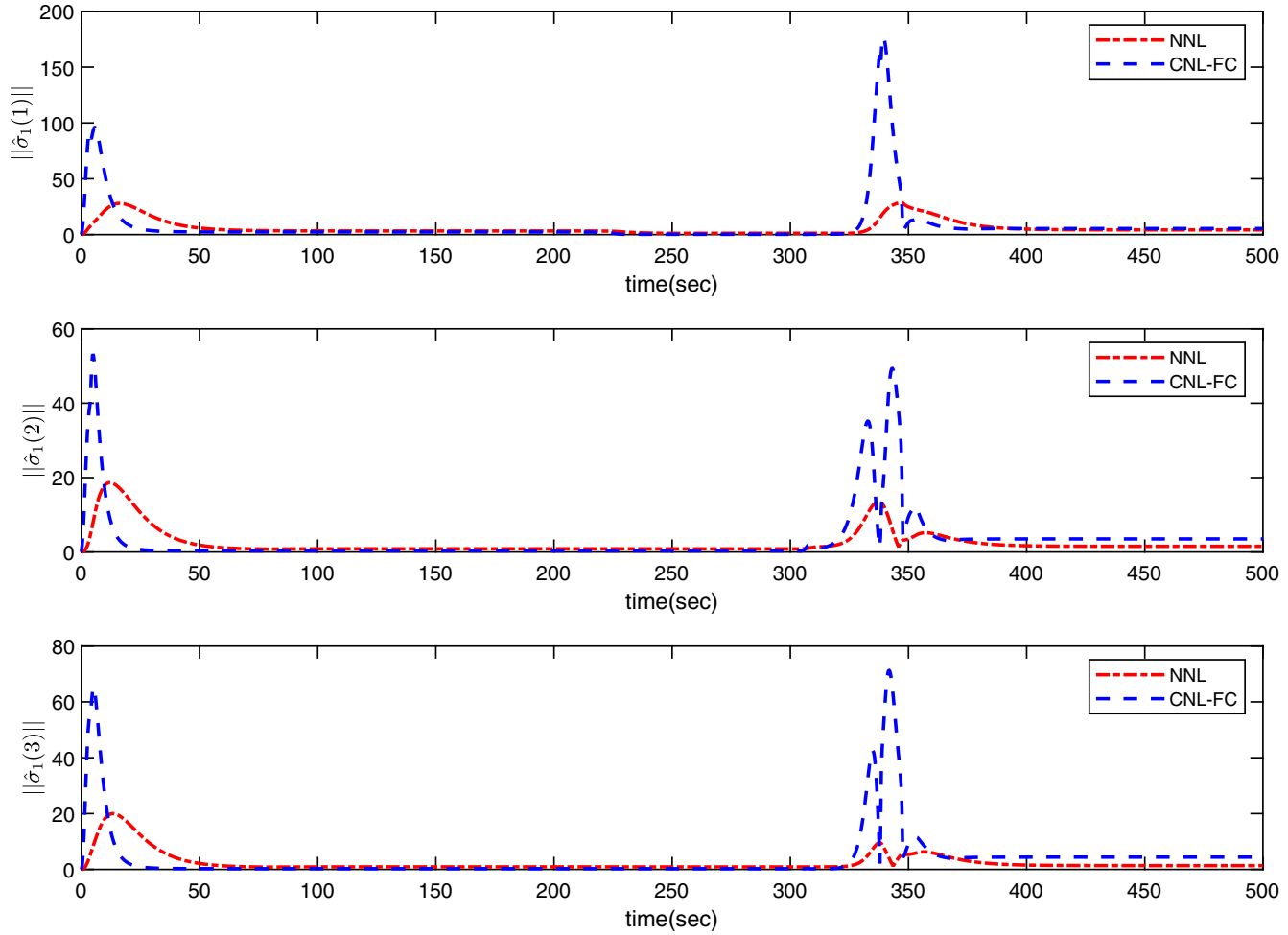

FIGURE 13 Trajectories of NN weights norm $\|\hat{\sigma}_1\|$ under "CNL-FC" method and "NNL" method [Colour figure can be viewed at wileyonlinelibrary.com]

time under ”CNL-FC” mehod. In Figure 13, the response of the neural weights norm $\|\hat{\sigma}_1\|$ under “CNL-FC” method sensitive to the dynamics uncertainties, because the prediction error χ_1 provides more feedback information for the neural update law.

In summary, it is obvious that the high-precision tracking and effective obstacle avoidance are realized with the proposed control. The trajectories of ten AUVs in Figure 2, the distance between AUVs and obstacles in Figure 3, and the distance between AUVs in Figure 4display that the formation tracking and the obstacle avoidance functions are acquired with the coordinated adaptive controller. Figure 5 exhibits that the AUV system is stable in a finite time, while Figure 6 demonstrates that the tracking error is limited by the function $\boldsymbol{m}_{1i}$. Furthermore, the high adaptation to system uncertainty and the finite-time convergence of prediction error are shown in Figures 10 and 12, respectively.

7 | CONCLUSION

The formation tracking control with finite-time convergence and obstacle avoidance is proposed for uncertain MAS in the article. The effective formation coordination and obstacle avoidance are obtained by using virtual structure and APF, and the higher tracking precision is achieved with the finite-time back-stepping control. The neural learning technology is designed to approximate the dynamics uncertainty, the SPEM is established by the system dynamics to obtain the prediction error. Furthermore, the predefined performance control is used to comply with the system state constraint. The finite-time UUB stability of the error single is proven through rigorous Lyapunov analysis. A simulation on ten AUVs system confirms the better coordinated tracking and higher learning performance. In future works, the adaptive state observer,[32] the event-triggered control,[33] and the fixed-time control[34] can be employed in the control design. Furthermore, the MAS with stochastic noise[35] and the heterogeneous switched MAS[36] will be studied due to the engineering requirements.

ACKNOWLEDGMENTS

This work was supported by the National Natural Science Foundation of China (Grant Nos. 61933010, 62003180), Science and Technology on Space Intelligent Control Laboratory, (Grant No. HTKJ2020KL502005).

CONFLICT OF INTEREST

The authors declare no potential conflict of interests.

DATA AVAILABILITY STATEMENT

Research data are not shared.

ORCID

Bin Xu https://orcid.org/0000-0001-9115-4686

REFERENCES

1. Xuan L. Distributed optimisation based on multi-agent system for resource allocation with communication time-delay. *IET Control Theory Appl*. 2019;14(4):549-557.
2. Wu Y. Coordinated path planning for an unmanned aerial-aquatic vehicle (UAAV) and an autonomous underwater vehicle (AUV) in an underwater target strike mission. *Ocean Eng*. 2019;182:162-173.
3. Shi W, Song S, Wu C, Chen CLP. Multi pseudo Q-learning-based deterministic policy gradient for tracking control of autonomous underwater vehicles. *IEEE Trans Neural Netw Learn Syst*. 2019;30(12):3534-3546.
4. Li R, Yang H, Xiao C. Cooperative hunting strategy for multi-mobile robot systems based on dynamic hunting points. *Control Eng Chian*. 2019;26(3):510-514.
5. Guerrero J, Torres J, Creuze V, Chemori A. Adaptive disturbance observer for trajectory tracking control of underwater vehicles. *Ocean Eng*. 2020;200:107080. https://doi.org/10.1016/j.oceaneng.2020.107080;200:107080.
6. Zhai X, Wen G, Peng Z, Zhang X. Leaderless and leader-following fixed-time consensus for multiagent systems via impulsive control. *Int J Robust Nonlinear Control*. 2020;30(13):5253-5266.
7. Li J, Zhang X, Zhang H, Du X. Trajectory tracking control of multi-AUVs formation based on virtual leader. Paper presented at: Proceedings of the 2019 IEEE Inyernational Conference on Mechatronics and Automation (ICMA); Tianjin, China; 2019:291-296.
8. He B, Ren H, Kan W. Design and simulation of behavior-based reactive decision-making control system for autonomous underwater vehicle. Paper presented at: Proceedings of the 2nd IEEE International Conference on Advanced Computer Control (ICACC 2010); Shenyang, China; Vol. 5, 2010:647-651.

9. Leonard NE, Fiorelli E. Virtual leaders, artificial potentials and coordinated control of groups. Paper presented at: Proceedings of the 40th IEEE Conference on Decision and Control; Orlando, FL, USA; 2001:2968-2973.
10. Cifuentes S, Maria G-SJ, Jimenez J. Virtual fields and behaviour blending for the coordinated navigation of robot teams: some experimental results. *Expert Syst Appl*. 2015;42(10):4778-4796.
11. Pan W, Jiang D, Pang Y, Li Y, Zhang Q. A multi-AUV formation algorithm combining artificial potential field and virtual structure. *Acta Armamentarii*. 2017;38(2):326-334.
12. Xie T, Li Y, Jiang Y, An L, Wu H. Backstepping active disturbance rejection control for trajectory tracking of underactuated autonomous underwater vehicles with position error constraint. *Int J Adv Robot Syst*. 2020;17(2). https://doi.org/10.1177/1729881420909633.
13. Bin Y, Xiao W, Yin H, Zhou Q, Lu R. Adaptive neural control for multiagent systems with asymmetric time-varying state constraints and input saturation. *Int J Robust Nonlinear Control*. 2020;30(12):4764–4778.
14. Wang J, Duan Z. A performance region-based approach to the leader-following consensus of nonlinear multiagent systems. *Int J Robust Nonlinear Control*. 2021;3(6):2168–2185.
15. Wang H, Liu S, Yang X. Adaptive neural control for non-strict-feedback nonlinear systems with input delay. *Inf Sci*. 2020;514:605-616.
16. Chen W, Hua S, Zhang H. Consensus-based distributed cooperative learning from closed-loop neural control systems. *IEEE Trans Neural Netw Learn Syst*. 2015;26(2):331-345.
17. Chen Q, Xie S, Sun M, He X. Adaptive nonsingular fixed-time attitude stabilization of uncertain spacecraft. *IEEE Trans Aerosp Electron Syst*. 2018;54(6):2937-2950.
18. Li Y, Min X, Tong S. Adaptive fuzzy inverse optimal control for uncertain strict-feedback nonlinear systems. *IEEE Trans Fuzzy Syst*. 2020;28(10):2363-2374.
19. Wang L, Wang H, Liu PX. Adaptive fuzzy finite-time control of stochastic nonlinear systems with actuator faults. *Nonlinear Dynamics*. 2021;104(1):523–536.
20. Zou W, Shi P, Xiang Z, Shi Y. Finite-time consensus of second-order switched nonlinear multi-agent systems. *IEEE Trans Neural Netw Learn Syst*. 2020;31(5):1757-1762.
21. Xu B, Wang X, Chen W, Shi P. Robust intelligent control of SISO nonlinear systems using switching mechanism. *IEEE Trans Cybern*. 2020. https://doi.org/10.1109/TCYB.2020.2982201.
22. Xu B, Shou Y, Luo J, Pu H, Shi Z. Neural learning control of strict-feedback systems using disturbance observer. *IEEE Trans Neural Netw Learn Syst*. 2019;30(5):1296-1307.
23. Cui B, Xia Y, Liu K, Shen G. Finite-time tracking control for a class of uncertain strict-feedback nonlinear systems with state constraints: a smooth control approach. *IEEE Trans Neural Netw Learn Syst*. 2020;31(11):4920–4932.
24. Li Y, Yang T, Liu L, Feng G, Tong S. Finite-time optimal control for interconnected nonlinear systems. *Int J Robust Nonlinear Control*. 2020;30(8).
25. Wang H, Bai W, Zhao X, Liu PX. Finite-time-prescribed performance-based adaptive fuzzy control for strict-feedback nonlinear systems with dynamic uncertainty and actuator faults. *IEEE Trans Cybern*. 2021. https://doi.org/10.1109/TCYB.2020.3046316.
26. Zhao L, Liu G, Yu J. Finite-time adaptive fuzzy tracking control for a class of nonlinear systems with full-state constraints. *IEEE Trans Fuzzy Syst*. 2020. https://doi.org/10.1109/TFUZZ.2020.2996387.
27. Min H, Xu S, Zhang Z. Adaptive finite-time stabilization of stochastic nonlinear systems subject to full-state constraints and input saturation. *IEEE Trans Autom Control*. 2021;66(3):1306–1313.
28. Shou Y, Xu B, Zhang A, Mei T. Virtual guidance-based coordinated tracking control of multi-autonomous underwater vehicles using composite neural learning. *IEEE Trans Neural Netw Learn Syst*. 2021. https://doi.org/10.1109/TNNLS.2021.3057068.
29. Yu J, Peng S, Lin Z. Finite-time command filtered backstepping control for a class of nonlinear systems. *Automatica*. 2018;92:173-180.
30. Xu B, Shou Y. Composite learning control of MIMO systems with applications. *IEEE Trans Ind Electron*. 2018;65(8):6414-6424.
31. Levant A. Robust exact differentiation via sliding mode technique. *Automatica*. 1998;34(3):379-384.
32. Mao J, Karimi HR, Xiang Z. Observer-based adaptive consensus for a class of nonlinear multiagent systems. *IEEE Trans Syst Man Cybern Syst*. 2019;49(9):1893-1900.
33. Zou W, Shi P, Xiang Z, Shi Y. Consensus tracking control of switched stochastic nonlinear multiagent systems via event-triggered strategy. *IEEE Trans Neural Netw Learn Syst*. 2020;31(3):1036-1045.
34. Song G, Shi P, Agarwal RK. Fixed-time sliding mode cooperative control for multiagent networks via event-triggered strategy. *Int J Robust Nonlinear Control*. 2021;31(1):21–36.
35. Wei Q, Wang X, Zhong X, Wu N. Consensus control of leader-following multi-agent systems in directed topology with heterogeneous disturbances. *IEEE/CAA J Automat Sin*. 2021;8(2):423431.
36. Zou W, Ki CA, Xiang Z. Fuzzy-approximation-based distributed fault-tolerant consensus for heterogeneous switched nonlinear multiagent systems. *IEEE Trans Fuzzy Syst*. 2021. https://doi.org/10.1109/TFUZZ.2020.3009730.

How to cite this article: Shou Y, Xu B, Lu H, Zhang A, Mei T. Finite-time formation control and obstacle avoidance of multi-agent system with application. *Int J Robust Nonlinear Control*. 2021;1–19. https://doi.org/10.1002/rnc.5641